JBC RESEARCH ARTICLE COLLECTION: BIOLOGY AND CHEMISTRY OF G PROTEIN-COUPLED RECEPTORS

Functional profiling of the G protein-coupled receptor C3aR1 reveals ligand-mediated biased agonism

Received for publication, July 20, 2023, and in revised form, November 21, 2023 Published, Papers in Press, December 10, 2023,
https://doi.org/10.1016/j.jbc.2023.105549

Pedro Rodriguez[1,‡], Lauren J. Laskowski[2,‡], Jean Pierre Pallais[1], Hailey A. Bock[2], Natalie G. Cavalco[2], Emilie I. Anderson[2], Maggie M. Calkins[2], Maria Razzoli[1], Yuk Y. Sham[1], John D. McCorvy[2,*], and Alessandro Bartolomucci[1,*]

From the [1]*Department of Integrative Biology and Physiology, University of Minnesota, Minneapolis, Minnesota, USA;* [2]*Department of Cell Biology, Neurobiology and Anatomy, Medical College of Wisconsin, Milwaukee, Wisconsin, USA*

Reviewed by members of the JBC Editorial Board. Edited by Kirill Martemyanov

G protein-coupled receptors (GPCRs) are leading druggable targets for several medicines, but many GPCRs are still untapped for their therapeutic potential due to poor understanding of specific signaling properties. The complement C3a receptor 1 (C3aR1) has been extensively studied for its physiological role in C3a-mediated anaphylaxis/inflammation, and in TLQP-21-mediated lipolysis, but direct evidence for the functional relevance of the C3a and TLQP-21 ligands and signal transduction mechanisms are still limited. In addition, C3aR1 G protein coupling specificity is still unclear, and whether endogenous ligands, or drug-like compounds, show ligand-mediated biased agonism is unknown. Here, we demonstrate that C3aR1 couples preferentially to Gi/o/z proteins and can recruit β-arrestins to cause internalization. Furthermore, we showed that in comparison to $C3a_{63-77}$, TLQP-21 exhibits a preference toward Gi/o-mediated signaling compared to β-arrestin recruitment and internalization. We also show that the purported antagonist SB290157 is a very potent C3aR1 agonist, where antagonism of ligand-stimulated C3aR1 calcium flux is caused by potent β-arrestin-mediated internalization. Finally, ligand-mediated signaling bias impacted cell function as demonstrated by the regulation of calcium influx, lipolysis in adipocytes, phagocytosis in microglia, and degranulation in mast cells. Overall, we characterize C3aR1 as a Gi/o/z-coupled receptor and demonstrate the functional relevance of ligand-mediated signaling bias in key cellular models. Due to C3aR1 and its endogenous ligands being implicated in inflammatory and metabolic diseases, these results are of relevance toward future C3aR1 drug discovery.

G protein-coupled receptors (GPCRs) are the largest superfamily of transmembrane proteins and are important targets for several diseases and disorders (1–3). Ligand binding triggers conformational changes that enable binding and activation of G proteins (4, 5) and dissociation of Gα and Gβγ subunits, each becoming downstream effectors (4–6). Phosphorylation of GPCRs by G protein-coupled receptor kinases (GRKs) enables β–arrestin binding, receptor internalization, and activation of downstream signaling pathways (7). Understanding GPCR signaling has evolved to include ligand-mediated biased signaling (5, 8, 9), a phenomenon by which a ligand stimulates signaling through one signal transducer over another (*e.g.*, β-arrestin *versus* G protein) (10). Biased signaling is an established concept and shows therapeutic value (11–13). Yet, our understanding of the mechanism of biased signaling is mostly informed by synthetic ligands, and limited knowledge of its physiological role exists without knowledge of endogenous biased ligand profiles (9, 14).

Complement 3a receptor (C3aR1) is a peptide-activated GPCR expressed in many cellular types including macrophages, mast cells, endothelial cells, adipocytes, and others (15–18). Reports described G protein coupling-specificity by C3aR1 to include Gi/o ((15) including Gi2 (19)), Gq (20), Gs (21), G12, and G13 (22). Yet a conclusive investigation into C3aR1 G protein coupling preferences is still lacking due to the lack of direct functional assays for this receptor. Furthermore, increasing literature about the role of the β-arrestin pathway and C3aR1 is emerging where both β-arrestin1 and β-arrestin2 can decrease ERK1/2 activation by C3aR1 (23, 24). GRKs phosphorylate and β-arrestins interact via phosphorylated serine and threonine residues on GPCRs like C3aR1 (23, 25). There is evidence that C3aR1 participates in multiple signaling pathways (17). For example, (i) the Wnt and β-catenin pathway by aiding tumor proliferation and cell migration (26); (ii) the GSK3β signaling pathways by helping to regulate tau phosphorylation (27); (iii) the p38 pathway in microglia to modulate pain (28); and (iv) the CAMKII/MAPK/ERK pathway to regulate lipolysis in adipocytes (29–31).

There are two known endogenous ligands identified for C3aR1, C3a, and TLQP-21 (17, 32). C3a is generated during alternative pathway activation when the C3 convertase cleaves C3 (15). Evolutionarily, the C3a peptide is highly conserved (17), and it may have evolved as an antimicrobial and antifungal peptide (33, 34). C3a is involved in inflammatory responses (15, 35), contraction of smooth muscle and vasodilation (36), and has a high binding affinity to IgE receptors which are found in mast cells (15). Additionally, C3a has been implicated in neurodegeneration (37) and can be

‡ Co-first authors.
* For correspondence: Alessandro Bartolomucci, abartolo@umn.edu; John D. McCorvy, jmccorvy@mcw.edu.

found in serum and can be a useful cancer biomarker (38). Unlike C3a, TLQP-21 is not regarded as a member of the complement system or as a classical immune-related peptide. TLQP-21 is produced upon proteolytic cleavage from the propeptide precursor VGF (nonacronymic), a member of the granin family of peptides (39). TLQP-21 protein can be detected in the central nervous system, peripheral nervous system, including the sympathetic nerve terminal in the adipose tissue, and the adrenal medulla (28, 30, 40). Intracerebroventricular infusion of TLQP-21 prevents the onset of obesity by increasing energy expenditure (40, 41); its peripheral injection exerts an anti-obesity effect (29, 41), increases adrenergic lipolysis (29, 42), modulates blood pressure (43), and improves pancreatic beta cell function (21). Thus, the field is split between the largely detrimental effects attributed to C3a, and the largely beneficial effects exerted by TLQP-21, yet the mechanisms for this dichotomous effect by these two ligands are currently unknown. The multifaceted role of C3aR1 in physiology is further highlighted by the unresolved pharmacology of SB290157, a putative C3aR1 antagonist (31, 44) also shown to exert agonist activity in some cellular models (45, 46).

Due to C3a and TLQP-21 being potential disease biomarkers, and C3aR1 being found in so many different tissues, there is an increasing importance in having clearly defined pharmacological mechanisms. Presently, there is a lack of direct functional assays detailing G protein coupling information for C3aR1. Also, little is known about biased ligand pharmacology at C3aR1 that can affect transducer-specific signaling pathways. In this study, we aim to characterize C3aR1 coupling preferences and investigate ligand-mediated C3aR1 signaling bias using endogenous agonists and other available C3aR1 ligands including the purported C3aR1 antagonist SB290157. We established that C3aR1 ligand-mediated signaling bias has functional significance in calcium influx, adipocyte, macrophage, and mast cell function. Due to C3aR1 and its endogenous ligands being implicated in several diseases, these results are of relevance toward drug discovery for this receptor.

Results

Profiling the transducerome reveals C3aR1 couples preferentially to Gi/o/z G protein subtypes

First, we aimed to determine which G protein subtypes are involved in C3aR1 signaling by testing a panel of Gα subtypes to couple to C3aR1 using a BRET platform in HEKT293 cells (47). Upon activation of C3aR1, this assay measures the loss of a BRET signal via G protein dissociation between the Gα-Rluc8 and Gβγ-GFP^2 (Fig. 1*A*). From a full screen panel of Gα proteins at C3aR1, our results reveal that Gi/o/z subtypes showed the most potent and efficacious G protein dissociation activities upon $C3a_{63-77}$-agonist (corresponding to the WWGKKYRASKLGLAR analogue of the C-terminal 15 amino acids of C3a (48)) stimulation, with no coupling activities detected for Gs, Gq or $G_{12/13}$ subtypes (Fig. 1*B*). C3aR1 coupling-specificities were confirmed in BRET experiments with empty pcDNA3.1 and no C3aR1 co-expressed, where $C3a_{63-77}$ was unable to elicit a net BRET G protein dissociation response at any of the tested G protein heterotrimer transducers (Fig. S1*A*). Among Gi/o/z subtypes, $C3a_{63-77}$ was most potent and efficacious for the Gi3 subtype (EC_{50} = 8.3 nM; net BRET = 0.32) followed by similar potency but slightly lower efficacy at activating GoA, GoB, and Gi1 subtypes. The weakest coupling for $C3a_{63-77}$-stimulated C3aR1 was detected for Gi2 and Gz (Fig. 1*C*). Next, we screened both human and mouse TLQP-21 (hTLQP-21 and mTLQP-21) for G protein dissociation activity at the Gi/o/z subtypes. We found that hTLQP-21 has a similar preference for GoA, GoB, and Gi1 over Gi2 and Gz subtypes, but hTLQP-21 shows ∼50-fold lower potency and lower efficacy to activate C3aR1 (Gi3 EC_{50} = 416 nM) compared to $C3a_{63-77}$ (Fig. 1, *D* and *E*). Similarly, mTLQP-21 also showed a preference for activating GoA, GoB, and Gi1 over Gi2 and Gz subtypes, but was more potent (Gi3 EC_{50} = 131 nM) compared to hTLQP-21. This mouse-over-human TLQP-21 difference in potency is consistent with our previous study measuring β-arrestin2 recruitment using the Tango assay platform (31). Taken together, our data demonstrate that C3aR1 primarily couples to the Gi/o/z subtypes but exhibits no significant coupling to Gs, Gq, or $G_{12/13}$ subtypes (Fig. 1*F*).

C3aR1 couples to Gi/o-proteins to inhibit cAMP accumulation

To confirm C3aR1-mediated Gi/o/z signaling, we performed cAMP inhibition measurements using Glosensor in HEKT cells, stimulated either by isoproterenol (ISO), a β-adrenergic receptor agonist, or by forskolin (FSK), a direct activator of adenylyl cyclase (Fig. 2*A*). C3aR1 activation by $C3a_{63-77}$, hTLQP-21, or mTLQP-21 reliably inhibited cAMP stimulation by either ISO or FSK (Fig. S1, *B* and *C*). Compared to G protein dissociation assays using BRET, rank order of potency was similar for all three peptides in the cAMP inhibition assay, albeit with much increased potencies, with $C3a_{63-77}$ (EC_{50} = 0.089 nM) > mTLQP-21 (EC_{50} = 10.4 nM) > hTLQP-21 (EC_{50} = 107 nM) (Fig. 2*B*). When normalized to percent $C3a_{63-77}$ response, all peptides had a similar efficacy suggestive of amplification and receptor reserve in this system. To confirm C3aR1 coupling to Gi/o in the cAMP inhibition assay, cells were treated with pertussis toxin (PTX) to uncouple Gi/o proteins, which completely abolished cAMP inhibition responses for all peptides (Figs. 2*B* and S1*D*). Overall, these experiments confirm that C3aR1 couples to Gi/o subtypes leading to cAMP inhibition and that $C3a_{63-77}$ is more potent than either mouse and human TLQP-21 to inhibit ISO and FSK induced potentiation of cAMP.

C3aR1 recruits β-arrestin to cause internalization

To directly measure β-arrestin recruitment to C3aR1, we constructed a C3aR1 receptor fused to Rluc8 on the C-terminus and measured Venus-tagged β-arrestin2 recruitment using BRET in HEKT293T (Fig. 2*C*). This assay is preferred to previous measurements using the Tango assay (49) because it can be easily compared using the same time and temperature

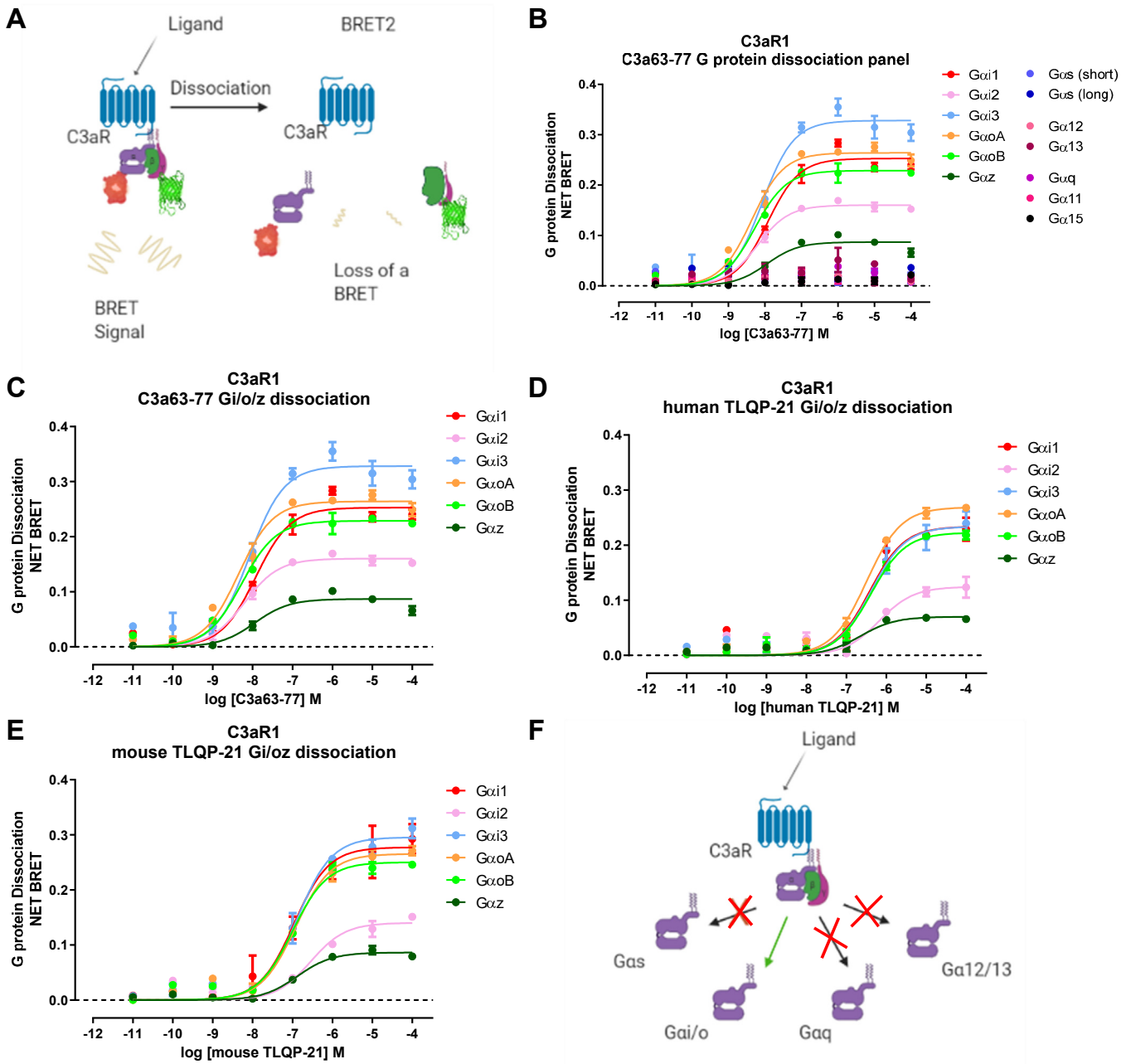

Figure 1. Profiling the transducerome reveals C3aR1 couples preferentially to Gi/o/z G protein subtypes. *A*, overview of transducer-wide C3aR1 G protein dissociation BRET assay. *B*, C3aR1 primarily couples to Gi/o/z G protein subtypes as measured by panel of G protein subtypes. Data represent net BRET effect on G protein dissociation and are the mean and SEM from three independent experiments. *C*, $C3a_{63-77}$-induced Gi/o/z dissociation as measured by BRET. *D*, hTLQP-21-induced Gi/o/z dissociation as measured by BRET. *E*, mTLQP-21-induced Gi/o/z dissociation as measured by BRET. *F*, summary of transducer profiling showing C3aR1 couples primarily to Gi/o/z subtypes and not to Gs, Gq, and G12/13 subtypes. Data represent net BRET response and are the mean and SEM from three independent experiments, which were performed at 37 °C with 60 min compound incubations.

conditions in G protein dissociation BRET (47) assays to assess ligand bias, and importantly, avoids overnight amplified transcriptional readout artifacts in the Tango system. In the BRET assay, C3aR1 robustly recruited β-arrestin1 and β-arrestin2 with GRK2 co-expression, and $C3a_{63-77}$ was highly potent to recruit β-arrestins in this assay (β-arrestin2 EC_{50} = 5.3 nM; Fig. 2*D*; β-arrestin1, EC_{50} = 5.4 nM; Fig. S1*E*). However, mTLQP-21 and hTLQP-21 were much less efficacious and potent to recruit β-arrestin2 in this assay compared to $C3a_{63-77}$, even when time and temperature conditions were the same as in G protein dissociation BRET assays (mTLQP-21 E_{max} = 46%; hTLQP-21 E_{max} = 52% of $C3a_{63-77}$ response). This result confirms and extend our previous data using the Tango assay (31, 50), demonstrating that $C3a_{63-77}$ is ∼100 times more potent at β-arrestin1 and β-arrestin2 recruitment when compared to mTLQP-21 (β-arrestin2 EC_{50} = 542 nM Fig. 2*D*; β-arrestin1 EC_{50} =191 nM Fig. S1*E*), and ∼1000 times more potent when compared to hTLQP-21 (β-arrestin2 EC_{50} = 3176 nM; Fig. 2*D*).

To confirm weaker C3aR1-mediated β-arrestin recruitment by mTLQP-21 compared to $C3a_{63-77}$, we measured β-arrestin-mediated internalization using an anti-FLAG ELISA assay in

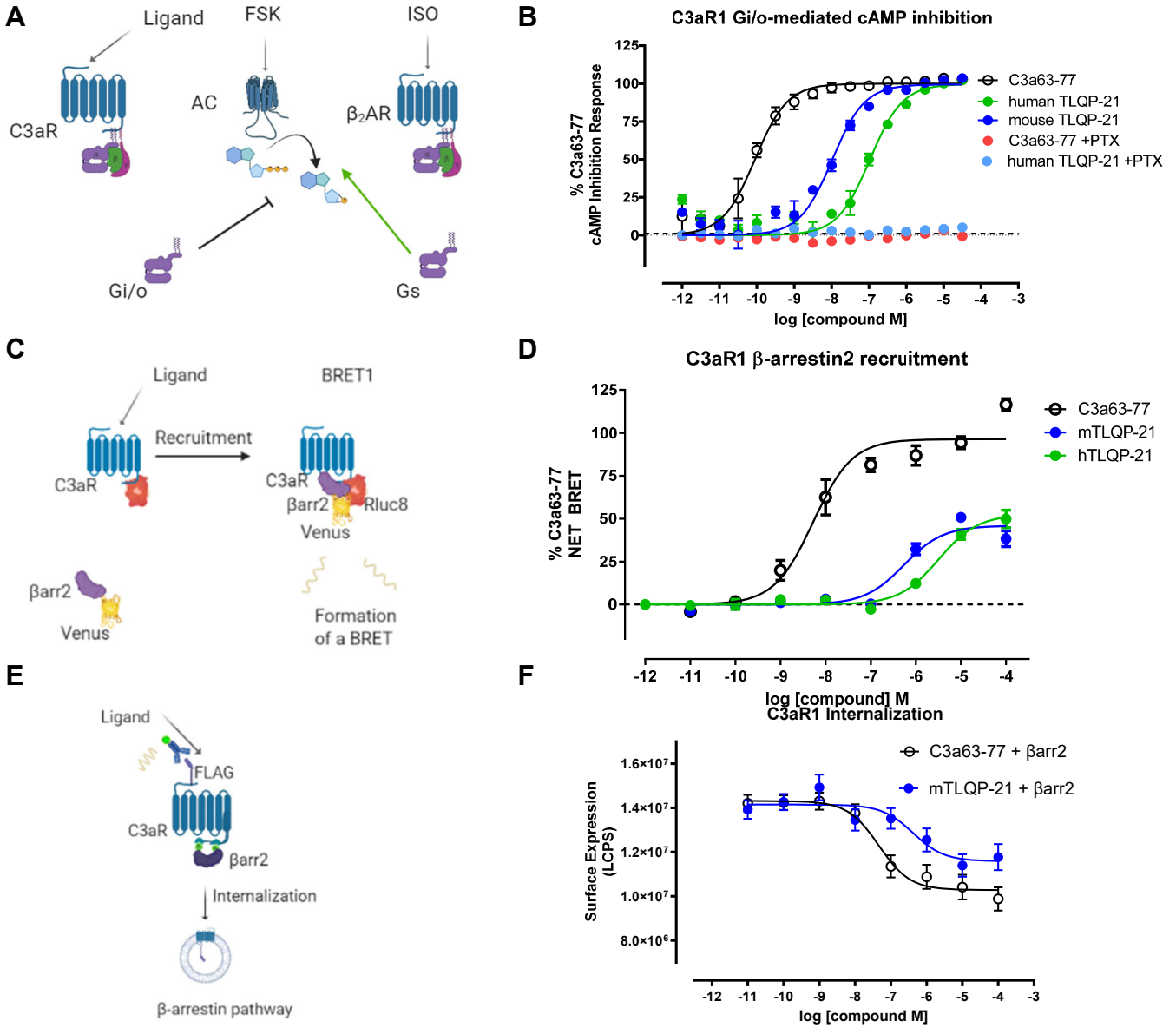

Figure 2. C3aR1 couples to Gi/o-proteins to inhibit cAMP accumulation and recruits β-arrestin to cause internalization. *A*, overview of C3aR1 activation of Gi/o to inhibit FSK or ISO-stimulated cAMP accumulation. *B*, C3aR1 Gi/o-mediated FSK-stimulated cAMP inhibition for $C3a_{63-77}$ (*open black circles*), human TLQP-21 (*green*), and mouse TLQP-21 (*blue*). Pertussis toxin (PTX)-treated cells to uncouple Gi/o proteins blocks $C3a_{63-77}$ (*red*) and human TLQP-21 (*light blue*)-mediated cAMP inhibition. Data represent percent $C3a_{63-77}$ response, and data are the mean and SEM from three independent experiments. *C*, overview of C3aR1 recruitment of β-arrestin2 as measured by BRET. *D*, C3aR1-mediated β-arrestin2 recruitment by BRET for $C3a_{63-77}$ (*open black circles*), human TLQP-21 (*green*), and mouse TLQP-21 (*blue*). Data represent the percentage of $C3a_{63-77}$ response, and data are the mean and SEM from three independent experiments, which were performed at 37 °C with 60 min compound incubations. *E*, overview of ELISA-based assay to measure FLAG-tagged C3aR1 receptor surface expression. *F*, C3aR1 β-arrestin2-mediated internalization as measured by ELISA for $C3a_{63-77}$ and mouse TLQP-21. Data represent surface expression as expressed as luminescence counts per second (LCPS), and data are the mean and SEM from three independent experiments, which were performed at 37 °C with 60 min compound incubations prior to tissue fixation.

non-permeabilized HEKT293T cells co-expressing C3aR1, GRK2, human β-arrestin2 (Fig. 2*E*), conditions similar to BRET assays. Again, $C3a_{63-77}$ caused a robust loss of C3aR1 surface expression (EC_{50} = 46 nM), but mTLQP-21 was much less potent and efficacious to cause internalization (EC_{50} = 416 nM; Fig. 2*F*). In ELISA experiments where β-arrestin2 was not co-expressed, both $C3a_{63-77}$ and mTLQP-21 failed to cause internalization, suggesting β-arrestin2 co-expression is necessary to detect internalization in this assay system (Fig. S1*F*).

Overall, these data confirm that C3aR1 activation leads to recruitment of β-arrestin2 and results in C3aR1 internalization and demonstrate that $C3a_{63-77}$ is much more potent and efficacious to recruit β-arrestin and internalize C3aR1 compared to mouse TLQP-21.

Profiling for C3aR1-biased agonism across Gi/o/z and β-arrestin2 transducers

To determine if human and mouse TLQP-21 exhibit ligand bias, as measured by preferences for either G protein dissociation *versus* β-arrestin2 recruitment, we compared all three peptides at G protein dissociation activity at all Gi/o/z

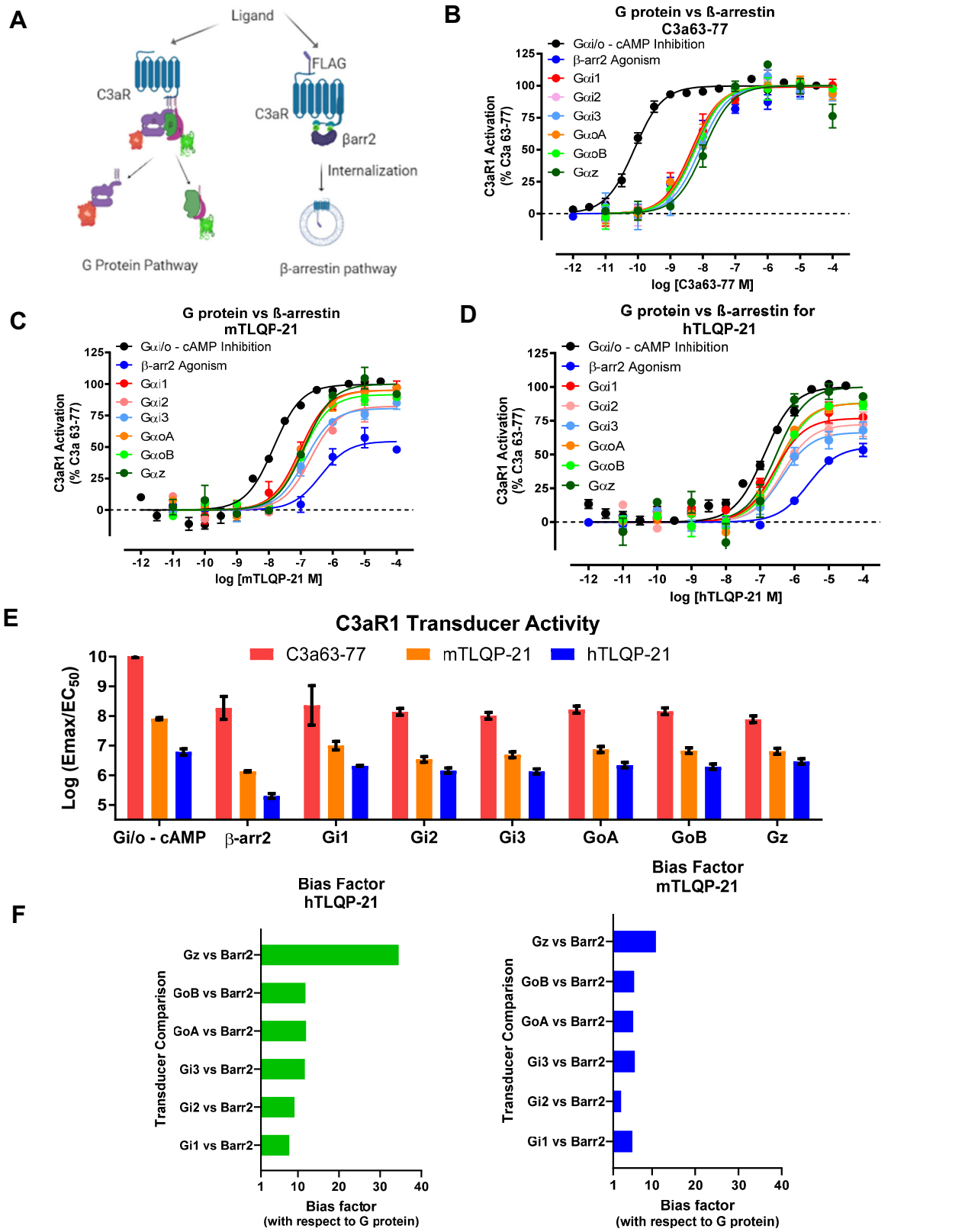

Figure 3. Profiling for C3aR1 biased agonism across Gi/o/z and β-arrestin2 transducers. *A*, overview of assays to measure G protein dissociation or β-arrestin2 recruitment activities for C3aR1. Comparison of all C3aR1 G protein *versus* β-arrestin2 activities for $C3a_{63-77}$ (*B*), mTLQP-21 (*C*), and hTLQP-21 (*D*). *E*, relative activities (log(E_{max}/EC_{50}) for G protein subtype dissociation or β-arrestin2 recruitment activities comparing $C3a_{63-77}$ (*red*), mTLQP-21 (*orange*), and hTLQP-21 (*blue*). *F*, comparisons of bias factors with respect to G protein subtype dissociation activity *versus* β-arrestin2 recruitment activity using $C3a_{63-77}$ as the reference ligand. Data represent the percentage $C3a_{63-77}$ response, and data are the mean and SEM from three independent experiments.

subtypes, Gi/o-mediated cAMP inhibition, and β-arrestin2 recruitment activities (Fig. 3*A*).

The peptide $C3a_{63-77}$ showed similar potency to cause Gi/o/z dissociation compared to β-arrestin2 recruitment but was much more potent in Gi/o-mediated cAMP inhibition, consistent with this system producing amplified responses with receptor reserve (Fig. 3*B*). However, both mouse and human TLQP-21 peptides were much weaker to recruit β-arrestin2 compared to their Gi/o/z dissociation or Gi/o-mediated cAMP inhibition potencies, suggesting TLQP-21 prefers Gi/o signaling over β-arrestin recruitment when compared to the $C3a_{63-77}$ peptide (Fig. 3, *C* and *D*). Importantly, a comparison of transduction coefficients [$\log(E_{max}/EC_{50})$] (51) indicates that both mouse and human TLQP-21 show the weakest activity for β-arrestin recruitment activity compared to all other signaling pathways (Fig. 3*E*). Formal calculation of bias factors using transduction coefficients (52) with respect to reference agonist $C3a_{63-77}$ revealed that both hTLQP-21 and mTLQP-21 exhibit G protein bias (range 3.4–35.1) for all the Gi/o/z subtypes relative to β-arr2 recruitment as measured by BRET (Fig. 3*F*). Overall our data confirm that both mTLQP-21 and hTLQP-21 exhibit preference for C3aR1 Gi/o signaling over β-arrestin recruitment compared to the balanced agonist $C3a_{63-77}$. However, mTLQP-21 is more potent compared to hTLQP-21, which is consistent with our previous study (31) and was therefore used for further experiments in cellular models.

C3aR1-mediated calcium influx responses in 3T3L1 cells are Gi/o-dependent

To confirm ligand-mediated C3aR1 signaling in cell lines other than HEK cells, we next focused on calcium influx, which is a major measured second messenger in response to C3aR1 activation in 3T3-L1 and other cells (17, 31, 50, 53). We compared $C3a_{63-77}$ and mTLQP-21-mediated Ca2+ influx in 3T3-L1 cells using single-cell live imaging-based Fluo4 assay (31). Using the Fluo-4 assay in 3T3-L1 cells, we confirmed that mTLQP-21 and $C3a_{63-77}$ have similar efficacy, but that $C3a_{63-77}$ is ∼100-fold more potent than mTLQP-21 at mobilizing calcium (Fig. 4*A*). Next, we measured the ability of pre-incubation (30 min followed by wash) of $C3a_{63-77}$ to block mTLQP-21-induced calcium influx. $C3a_{63-77}$ caused a dose dependent inhibition of TLQP-21(10 μM)-induced calcium

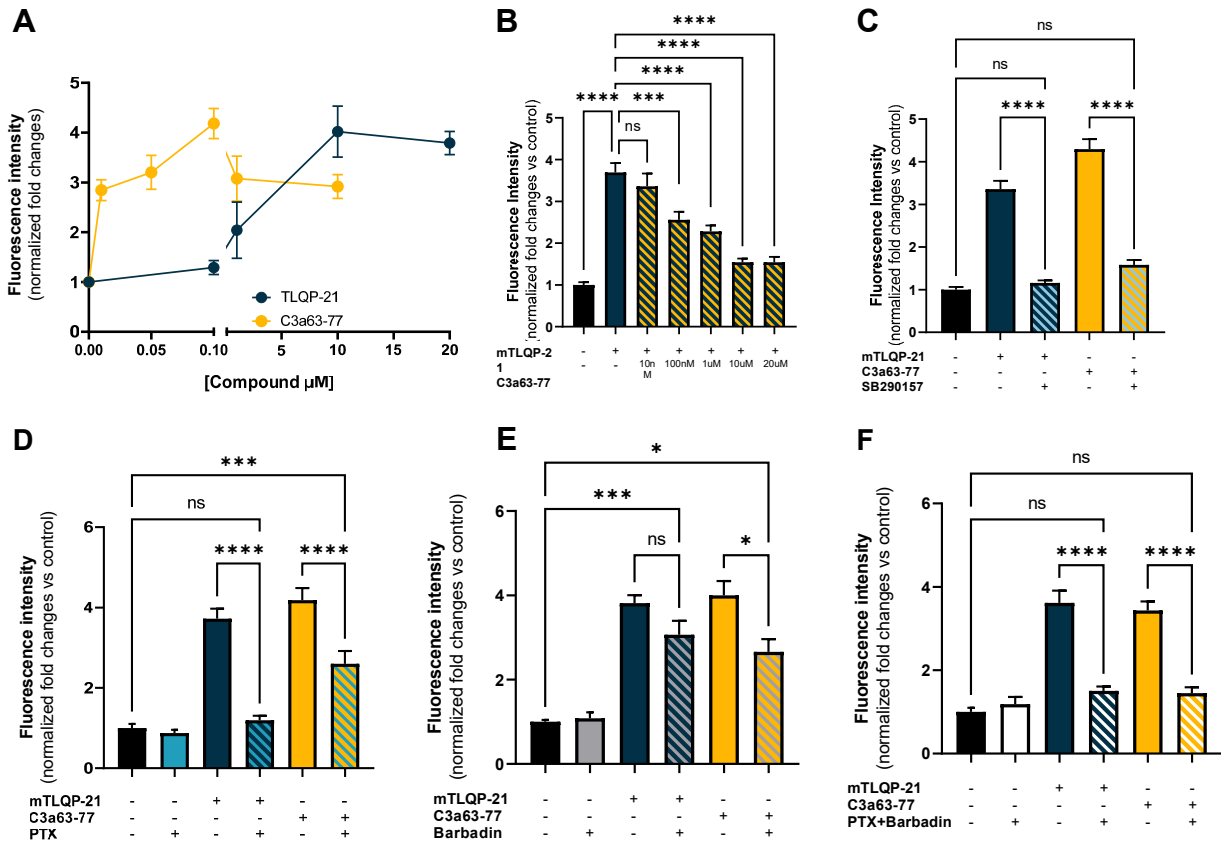

Figure 4. C3aR1-mediated calcium influx responses in 3T3L1 cells are Gi/o-dependent. *A*, $C3a_{63-77}$ is a more potent agonist than TLQP-21 at increasing [Ca^{2+}]i (as measured by Fluo-4) (N = 30–75 from six independent experiments). *B*, TLQP-21 (10 μM) increased [Ca^{2+}]i is dose dependently inhibited by pretreatment with $C3a_{63-77}$ ($F(6, 525) = 23.62$, $p < 0.0001$, N = 40–75 cells from three independent experiments). *C*, TLQP-21 (10 μM) and $C3a_{63-77}$ (100 nM) increased [Ca^{2+}]i is antagonized by SB290157 (20 μM) ($F(4, 304) = 79.1$, $p < 0.0001$, N = 25–89 from four independent experiments). *D*, PTX (1 μg/ml) fully inhibits TLQP-21 (10 μM) induced increased of [Ca^{2+}]i, but only partially inhibits $C3a_{63-77}$ (100 nM) induced increase of [Ca^{2+}]i ($F(5, 265 = 29.42$, $p < 0.0001$, N = 24–70 from three independent experiments). *E*, Barbadin (100 μM) partially inhibits $C3a_{63-77}$ (100 nM) induced increase of [Ca^{2+}]i but not TLQP-21 (10 μM) ($F(5, 479) = 11.39$, $p < 0.0001$, N = 29–130 from four independent experiments). *F*, a combination of PTX (1 μg/ml) and Barbadin (100 μM) fully inhibits both TLQP-21 (10 μM) and $C3a_{63-77}$ (100 nM) induced increase of [Ca^{2+}]i ($F(6, 210) = 27.31$, $p < 0.0001$, N = 20–45 from two independent experiments). Tukey's multiple comparisons test, ns = not significant, *$p < 0.05$, **$p < 0.01$, ***$p < 0.001$, ****$p < 0.0001$.

influx (Fig. 4*B*), supporting competitive binding for the orthosteric site, receptor desensitization and internalization (Fig. 2*F*). Additionally, the purported C3aR1 antagonist, SB290157, was also capable of blocking $C3a_{63-77}$-mediated calcium influx (Fig. 4*C*). The presence of some residual receptor-bound orthosteric ligand after washing (31) could potentially compete with the effect exerted by a second orthosteric ligand, making it difficult to attribute the observed effects solely to internalized receptors. To address this limitation we performed next experiments in the presence of β-arrestin and endocytosis-mediated inhibitors.

Although both $C3a_{63-77}$ and TLQP-21 increase calcium mobilization, how C3aR1 activation regulates this calcium influx is unclear. To determine the degree of contribution of Gαi/o or β-arrestin on calcium influx, we utilized the Gi/o inhibitor PTX and the β-arrestin/AP2 endocytic complex inhibitor barbadin (54) measuring calcium influx using the Fluo-4 assay. TLQP-21 mediated calcium influx was abolished by pretreatment with PTX or PTX plus barbadin (Figs. 4*D* and *F* and S2*A*), whereas barbadin alone failed to inhibit calcium influx (Fig. 4*E*). Conversely, both PTX and barbadin significantly diminished, but did not completely abolish, $C3a_{63-77}$ mediated calcium influx (Fig. 4, *D* and *E*), whereas PTX/barbadin combination was required to completely abrogate calcium influx back to basal levels (Fig. 4*F*). The requirement of receptor internalization for β-arrestin-mediated C3aR1 signaling suggested by the inhibitory effect of barbadin, was confirmed using the endocytosis inhibitor Pitstop-2 (55) (Fig. S2, *B* and *C*).

Overall, in a cell line where C3aR1 is natively expressed, $C3a_{63-77}$ elicits calcium influx via multiple signaling pathways downstream of C3aR1, whereas mTLQP-21-mediated calcium influx is completely Gi/o dependent.

Functional significance of ligand-mediated C3aR1 signaling in 3T3 cells

Since our data demonstrate that $C3a_{63-77}$ is a more potent C3aR1 agonist than mTLQP-21, we hypothesized that it would potentiate adrenergic-mediated lipolysis to a greater degree than mTLQP-21. We first confirmed that C3aR1 activation elicits calcium flux in 3T3-L1 differentiated adipocytes. Consistent with the effect in undifferentiated fibroblasts, both mTLQP-21 and $C3a_{63-77}$ induced a dose-dependent increase in calcium influx with similar efficacy, although $C3a_{63-77}$ was ∼100 fold more potent (Fig. S3*A*). This influx can be pharmacologically inhibited by SB290157 (Fig. S3*B*) and requires C3aR1 expression, as suggested by absence of calcium influx in C3aR1-KD 3T3-L1 (31) (Fig. S3*C*).

Next, 3T3-L1 adipocytes were incubated with various concentrations of either mTLQP-21 or $C3a_{63-77}$ at either 3 h or 30 min incubation time. Despite $C3a_{63-77}$ being more potent than mTLQP-21 at C3aR1 activation (Figs. 1–3) and calcium influx (Fig. 4*A*), $C3a_{63-77}$ and mTLQP-21 were similar in their degree to potentiate adrenergic-induced lipolysis (Fig. 5, *A* and *B*), with SB290157 inhibiting ligand-induced lipolysis (Fig. S3, *D* and *E*). In line with the requirement of Gi/o for mTLQP-21 mediated calcium influx, PTX or PTX+barbadin pretreatment abrogated mTLQP-21 (100 nM) potentiation of adrenergic-induced lipolysis (3 h incubation. Fig. 5, *C* and *D*). Conversely, PTX alone did not inhibit $C3a_{63-77}$ (100 nM) mediated potentiation of adrenergic-induced lipolysis, while the combination of PTX+barbadin was sufficient to prevent $C3a_{63-77}$ potentiation of adrenergic-induced lipolysis (3 h incubation, Fig. 5, *C* and *D*). Finally, the endocytosis inhibitor Pitstop-2 exerted a similar effect on ligand induced lipolysis as shown by barbadin (Fig. S3*F*). Overall, these results establish the functional relevance of G protein *versus* β-arrestin contributions of $C3a_{63-77}$ and mTLQP-21 toward the potentiation of lipolysis in adipocytes.

Functional significance of ligand-mediated C3aR1 signaling in BV2 and LAD2 cells

Next, we aimed to extend our functional characterization to other murine and human cell lines natively expressing C3aR1, used previously to study the pharmacology and physiology of this pathway (56, 57): BV2, a mouse microglia-derived cell line (58) and LAD2, a human mast cell line (59).

The ability of $C3a_{63-77}$ and mTLQP-21 to act as agonists in calcium influx is conserved in BV2 cells (Fig. S4*A*). Furthermore, TLQP-21 mediated calcium influx in BV2 cells can be inhibited by SB290157 (Fig. S4*B*), by the TRPC blocker SKF 96365 (Fig. S4*C*) and by PTX (Fig. S4*D*). Similar to lipolysis in 3T3-L1, $C3a_{63-77}$ and mTLQP-21 were comparable in their degree at eliciting phagocytosis in BV2 cells at 1 μM concentrations (Fig. S4*E*).

The ability of $C3a_{63-77}$ and mTLQP-21 to act as agonists in calcium influx is also conserved in LAD2 cells (Fig. S5*A*). Unlike in 3T3-L1 and BV2 cells, $C3a_{63-77}$ retained higher potency and efficacy in a wide dose-range than mTLQP-21 in the β-hexosaminidase secretion assay in LAD2 cells (Fig. S5*B*).

Purported antagonist SB290157 is a pan-agonist at all C3aR1 transducer signaling pathways

SB290157 is widely used as a C3aR1 antagonist (31, 44, 60, 61). However, some reports identify this compound as showing C3aR1 agonism as well (45, 46). Based on our C3aR1 transducer and signaling analysis, we next interrogated the pharmacology of SB290157 using full-screen panel of Gα proteins at C3aR1, measuring G protein dissociation by BRET. Surprisingly, SB290157 showed robust C3aR1 G protein dissociation agonist activity across all tested Gi/o/z subtypes, but no activity at other G protein subtypes, similar to results with $C3a_{63-77}$ (Fig. 6*A*). SB290157 was able to activate Gi/o/z subtypes with a similar rank order of preference, but was ∼10-fold more potent to cause G protein dissociation compared to $C3a_{63-77}$ (Fig. 6*A*). We also confirmed SB290157 shows agonist activity in FSK-induced Gi/o-mediated cAMP inhibition in the Glosensor assay (Fig. 6*B*). Next, we tested SB290157 in β-arrestin1 and β-arrestin2 recruitment BRET assays and observed that SB290157 is also more potent than $C3a_{63-77}$ in this pathway (Fig. 6, *C* and *D*). Finally, SB290157 was also more potent and efficacious to induce β-arr2-dependent C3aR1

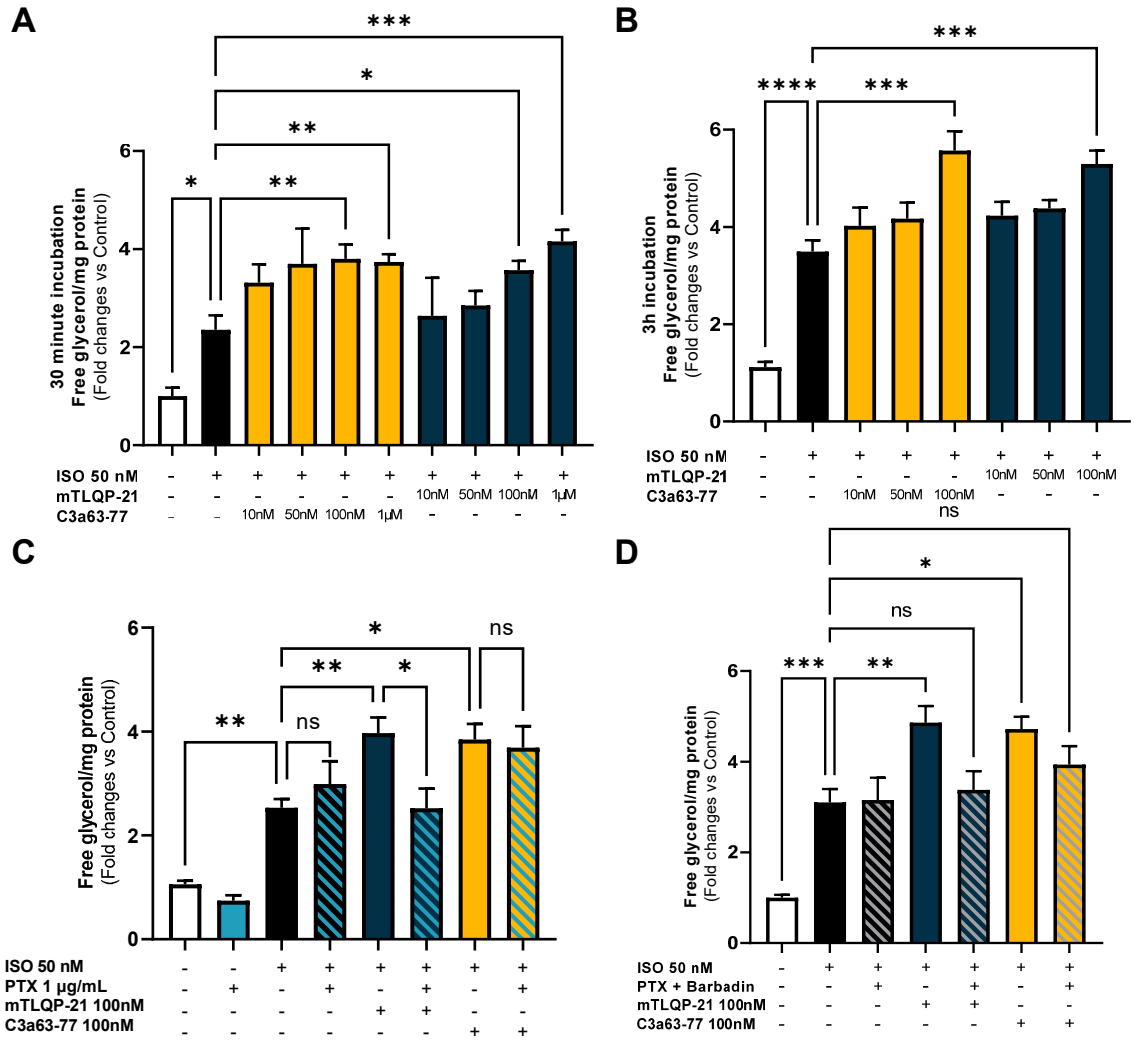

Figure 5. Functional significance of ligand-mediated C3aR1 signaling in 3T3L1 cells. *A* and *B*, dose-dependent effect of $C3a_{63-77}$ and TLQP-21 on potentiating isoproterenol (ISO)-induced lipolysis in 3T3-L1 derived adipocytes during a 30 min incubation period ($F(9,46) = 12.42$, $p < 0.0001$, N = 3–9), or a 3 h incubation period ($F(7, 70) = 20.08$, $p < 0.0001$, N = 7–12). *C*, PTX (1 μg/ml) inhibits TLQP-21 (100 nM) potentiation of ISO-induced lipolysis, but not $C3a_{63-77}$ (100 nM) ($F(8, 102) = 17.0$, $p < 0.0001$, N = 7–20). *D*, a combination of PTX (1 μg/ml) and Barbadin (100 μM) inhibits TLQP-21 (100 nM) potentiation of ISO-induced lipolysis, and prevents $C3a_{63-77}$ (100 nM) potentiation of ISO induced lipolysis ($F(10, 134) = 17.82$, $p < 0.0001$, N = 8–19 from two independent experiments). Tukey's multiple comparisons test, ns = not significant, *$p < 0.05$, **$p < 0.01$, ***$p < 0.001$, ****$p < 0.0001$.

internalization compared to $C3a_{63-77}$ (Fig. 6*E*). Across all C3aR1 measured transducers and signaling activities, SB290157 showed superior potency compared to $C3a_{63-77}$ but no preference for either G protein or β-arrestin recruitment activity (Fig. 6*F*). Collectively, these results demonstrate that SB290157 is a potent pan-agonist at all measured C3aR1 transducer signaling pathways.

Blockade of calcium influx by SB290157 is dependent on β-arrestin-induced internalization

Intriguingly, despite being a potent C3aR1 agonist, SB290157 does not induce calcium influx in 3T3-L1 (Figs. 4*C* and S3*B*), which is consistent with a previous study (60). Similarly, SB290157 did not elicit β-hexosaminidase release in LAD2 cells (Fig. S5*B*), and did not potentiate adrenergic-induced lipolysis in 3T3-L1 adipocytes (Fig. 6*G*).

To address these discrepancies in pharmacological activity, we focused on calcium influx and hypothesized that antagonism by SB290157 on mTLQP-21 and $C3a_{63-77}$ mediated calcium influx is mediated by its potent β–arrestin recruitment and ability to internalize C3aR1. Therefore, we preincubated 3T3-L1 cells with barbadin or Pitstop-2 to block β-arrestin-mediated internalization and challenged the cells with SB290157. In presence of barbadin or Pitstop-2, SB290157 was able to elicit an increase in calcium influx, thus showing C3aR1 agonist activity (Figs. 6*H* and S2*D*). SB290157's ability to interfere with C3aR1's calcium flux response via β-arrestin is further supported by barbadin's ability to limit SB290157 inhibition of TLQP-21-induced calcium influx (Fig. 6*I*).

Recently, JR14a was developed as an SB290157 derivative with increased potency (56). Consistently, JR14a was more potent than SB290157 at inhibiting mTLQP-21 mediated calcium influx in 3T3-L1 (Fig. S6*A*). Jr14a also inhibited

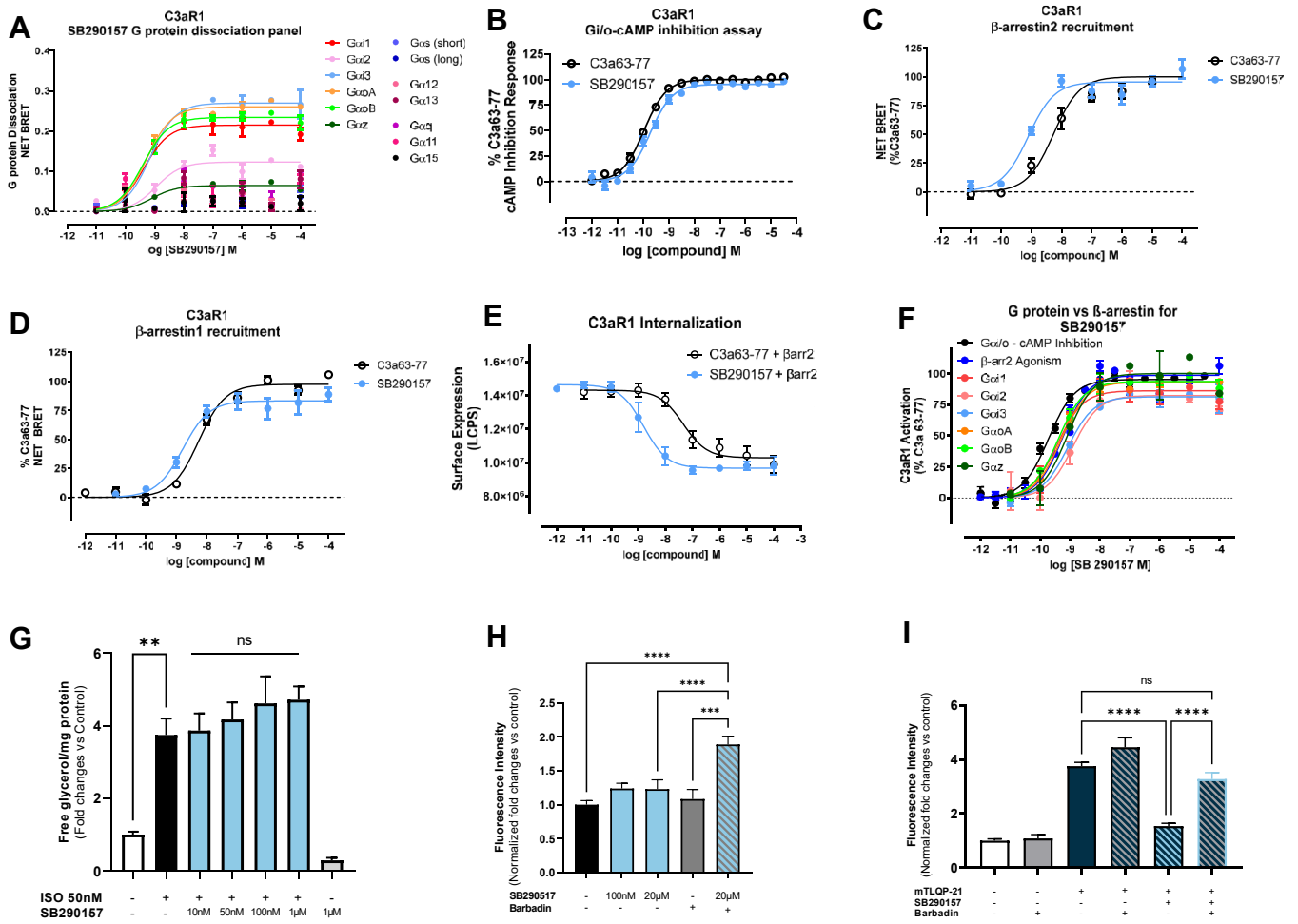

Figure 6. Purported antagonist SB290157 is a pan-agonist at all C3aR1 transducer signaling pathways. *A*, SB290157 shows pan-agonism at all Gi/o/z G protein subtypes but not Gs, Gq, or G12/13 subtypes as measured by panel of G protein subtypes. Data represent net BRET effect on G protein dissociation and are the mean and SEM from three independent experiments performed at 37 °C with 60 min compound incubations. *B*, comparison of Gi/o-mediated cAMP inhibition by SB290157 (*light blue*) and $C3a_{63-77}$ (*open black circles*). Data represent percent $C3a_{63-77}$ response, and data are the mean and SEM from three independent experiments. *C*, comparison of C3aR1-mediated β-arrestin2 recruitment by BRET by SB290157 (*light blue*) and $C3a_{63-77}$ (*open black circles*). Data represent percent $C3a_{63-77}$ response, and data are the mean and SEM from three independent experiments performed at 37 °C with 60 min compound incubations. *D*, C3aR β-arrestin1 recruitment activity as measured by BRET comparing SB290157 (*light blue*) to $C3a_{63-77}$ (*open black circles*). Data represent percent $C3a_{63-77}$ response, and data are the mean and SEM from three independent experiments. *E*, comparison of C3aR1-mediated internalization by SB290157 (*light blue*) and $C3a_{63-77}$ (*open black circles*). Data represent surface expression as expressed as luminescence counts per second (LCPS), and data are the mean and SEM from three independent experiments, which were performed at 37 °C with 60 min compound incubations prior to tissue fixation. *F*, comparison of all C3aR1 G protein *versus* β-arrestin2 activities for SB290157. Data represent percent $C3a_{63-77}$ response, and data are the mean and SEM from three independent experiments. *G*, SB290157 does not potentiate isoproterenol (ISO)-induced lipolysis in 3T3-L1 derived adipocytes regardless of concentration ($F(7,69) = 9.766$, $p < 0.0001$, N = 5–12). *H*, Barbadin (100 μM) treatment is permissive for SB290157 (20 μM) to induce $[Ca^{2+}]i$ ($F(3,270) = 13.95$, $p < 0.0001$, N = 30–110 from three independent experiments). SB290157 does not potentiate calcium influx in absence of barbadin. *I*, Barbadin (100 μM) rescues TLQP-21 (10 μM) increased $[Ca^{2+}]i$ in cells treated with SB290157 (20 μM) ($F(6, 757) = 55.33$, $p < 0.0001$, N = 100–222). Tukey's multiple comparisons test, ns = not significant, $*p < 0.05$, $**p < 0.01$, $***p < 0.001$, $****p < 0.0001$.

mTLQP-21-induced potentiation of adrenergic induced lipolysis (Fig. S6, *B* and *C*). In a similar fashion to SB290157, inhibiting β-arrestin mediated internalization with barbadin allows JR14a to act as an agonist in calcium influx (Fig. S6*D*) and prevents JR14a inhibition of TLQP-21 mediated calcium influx (Fig. S6*E*.

Taken together, our results support the conclusion that SB290157 is in fact a potent C3aR1 agonist, but that SB290157's ability to potently internalize C3aR1, prevents calcium influx in response to mTLQP-21 in the 3T3-L1 cell line, overall suggesting that SB290157-mediated β–arrestin activation and receptor internalization is the key mechanism for its calcium influx antagonism.

Discussion

GPCRs exhibit a wide range of signaling and coupling preferences, which complicates the understanding of their function, and exploitation of pharmacological targeting. This is particularly true for receptors like C3aR1, which has two endogenous ligands exerting seemingly different functional effects: largely detrimental C3a (anaphylaxis, inflammation, etc); largely beneficial TLQP-21 (anti-obesity, anti-diabetic, etc). Our study is the first to investigate the C3aR1 coupling transducerome and ligand-mediated C3aR1 biased signaling. Our work is one of the first on signaling bias of a complement receptor (62, 63), and one of the few examples of biased signaling by endogenous ligands (5, 64), the best characterized

being ligand and receptor-mediated biased MC4R signaling (64–66).

We showed that C3aR1 couples exclusively with the Gi/o/z family, with a slight subtype selectivity preference difference exerted by $C3a_{63-77}$, mTLQP-21, and hTLQP-21. Coupling to Gz was generally characterized by lower potency and efficacy than coupling to Gi/o subtypes. Consistent with Gi/o coupling, all peptides were unable to elicit cAMP inhibition when cells were exposed to PTX. Furthermore, $C3a_{63-77}$, mTLQP-21, and hTLQP-21, were most potent for cAMP inhibition compared to the β-arrestin pathway, but the TLQP-21 peptides exhibited degrees of partial agonism (67) compared to $C3a_{63-77}$.

We also sought to determine the pharmacological activity of SB290157 and whether it shows C3aR1 antagonist activity *in vitro* (31, 36, 56, 60, 68) or a C3aR1 agonist (45, 46). We unambiguously demonstrated that SB290157 activity elicited activation of Gi/o/z, β-arrestin recruitment, and inhibition of isoproterenol-induced cAMP—all C3aR1-mediated agonist effects. We also showed that SB290157 was the most potent ligand tested to induce β-arrestin mediated internalization. However, this was not a universal feature of this molecule, since $C3a_{63-77}$ showed higher potency at cAMP inhibition activity compared to SB290157. Yet, SB290157 was inactive in inducing calcium influx in 3T3-L1 cells or in eliciting functional activation of 3T3-L1 adipocytes or LAD2 mast cells. Importantly, we provide direct evidence that blocking C3aR1 internalization with barbadin (or Pitstop-2) was sufficient to unmask SB290157 agonism in the Fluo-4 calcium assay, and prevent its ability to inhibit ligand-induced calcium influx in 3T3-L1 cells. Overall, our data show that SB290157 is a C3aR1 agonist and that its antagonist effect on calcium flux is due to its potent β-arrestin mediated internalization preventing ligand binding and downstream signaling mediated by G protein activation. Thus, the reported agonist effects of this compound in some cell lines may be attributed to activation of β-arrestin-mediated signaling pathways (4, 24, 69).

In spite of conclusive evidence from several labs including ours that TLQP-21 and C3a (and its derivatives, like $C3a_{63-77}$) are C3aR1 agonists, it is remarkable that the field is split between the largely detrimental effects attributed to C3a and its analogues [anaphylaxis, hypertension, neurodegeneration (15, 35, 61, 70, 71)] and the largely beneficial effects exerted by TLQP-21 [anti-obesity, pro-lipolytic, anti-hypertensive, protective of β–cell loss and neurodegeneration (21, 29, 43). The only exception is a pro-nociceptive effect exerted by mTLQP-21 (28, 44, 72)]. A mechanistic understanding of this differential physiological effect exerted by the two peptides is still lacking. One possible explanation is a location and time-dependent difference in ligand activation: C3a is generated during the activation of the complement cascade (73); while TLQP-21 is secreted as a neuropeptide modulator from nerve terminals (30), and possibly endocrine glands (39). However, this explanation is likely partial, because most of the mechanistic studies were conducted *in vitro*, using cellular models and a full dose-range which should account for ligand concentrations occurring *in vivo*. Instead, our pharmacological investigation suggests that ligand-mediated signaling bias can contribute to the functional differences among C3aR1 endogenous ligands.

Focusing on metabolism, we and others established a positive association between C3aR1 expression in adipose and obesity in both humans (31, 74) and mice (29, 75, 76). Mechanistically, TLQP-21 elicits a C3aR1-dependent Ca2+ influx via TRPC channels leading to the activation of CaMKII/ERK (29–31). This signaling cascade is not lipolytic per se but potentiates βAR-induced lipolysis *in vitro* (29–31) and *in vivo* [(29, 42) and present study]. TLQP-21 also exerts an anti-obesity effect in mice and hamsters (29, 77) with a mechanism requiring C3aR1 and βAR (29). Knowledge on the role of C3a on metabolism is limited, unlike its established role in immunity (15, 35, 78, 79). C3a increases adipocyte differentiation (80) and inhibits forskolin-induced cAMP increase or βAR-induces lipolysis (81), with $C3a_{70-77}$ being less efficacious than TLQP-21 in potentiating ISO-induced lipolysis (29). Here, we showed that $C3a_{63-77}$ is several orders of magnitude more potent at cAMP inhibition, calcium influx, and β-arrestin recruitment than TLQP-21, yet it is not more potent in eliciting lipolysis in 3T3-L1. Similarly, SB290157 is more potent than TLQP-21 in all assays except for its inactivity in calcium influx and lipolysis in adipocytes. Taking data together, our data are consistent with the following mechanism (Fig. 7): (1). In the absence of βAR activation, C3aR1 activation elicits no lipolysis because cAMP inhibition and β–arrestin-mediated internalization opposes Gi/o-mediated increase in Ca2+ and downstream signaling (29–31); (2). In the presence of βAR activation, TLQP-21 mediates Gi/o-mediated increase in calcium, with minimal engagement of cAMP inhibition and β-arrestin recruitment, resulting in potentiation of βAR-induced lipolysis (29–31); (3) In the presence of βAR activation, $C3a_{63-77}$ elicits Gi/o induced cAMP inhibition and β–arrestin-mediated internalization which oppose Gi/o mediated calcium influx, resulting in concentration-dependent potentiation [(29) and current study], or inhibition (81), of βAR-induced lipolysis. (4) SB290157 prevents ligand mediated calcium influx due to strong β-arrestin mediated internalization, preventing TLQP-21 mediated potentiation of adrenergic induced lipolysis. To summarize, our data suggest a mechanistic explanation for the paradoxical equipotency of TLQP-21 and $C3a_{63-77}$ (which is nonetheless a more potent C3aR1 agonist) on lipolysis: Gi/o-mediated calcium flux prevails over cAMP inhibition and β-arrestin activation when compared to C3a, leaving the potentiation of adrenergic induced lipolysis unabated. The similar efficacy manifested by TLQP-21 and $C3a_{63-77}$ on BV2 cells in eliciting phagocytosis suggests a similar mechanism as observed in adipocytes on this cell function.

Interestingly, in mast cells, $C3a_{63-77}$ retained a significant potency difference when compared to mTLQP-21 in eliciting degranulation. Additionally, SB290157 was entirely inactive in eliciting degranulation in LAD2 cells. This result is in keeping with previous literature showing potent β–hexosaminidase release by $C3a_{63-77}$ (25, 48, 56, 82), and suggests that calcium influx (not elicited by SB290157) is required for mast cell degranulation. This result also suggests that a balanced agonist

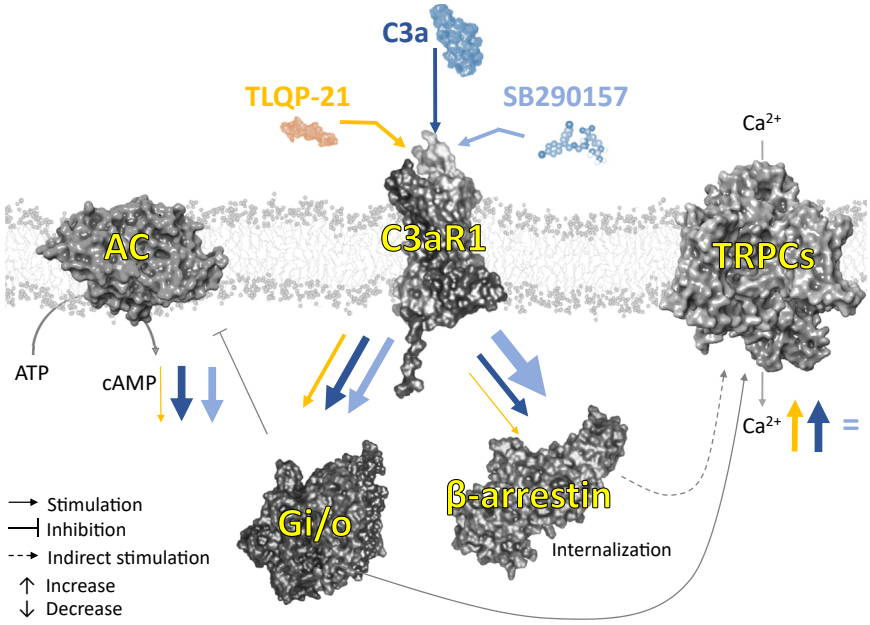

Figure 7. Summary of the proposed mechanism of ligand-mediated C3aR1 signaling bias. The cartoon shows the key molecules involved in the C3aR1 trasducerome and signaling pathway in adipocytes. The thickness of the arrows reflects the relative potency and/or efficacy described in the main figures. AC = Adenylyl cyclase, TRPCs = Transient receptor potential channels.

(like C3a) rather than a ligand preferentially activating Gi/o and calcium influx with minimal β–arrestin recruitment (like TLQP-21) is required to elicit full mast cell activation. This conclusion can have important therapeutic implication in developing C3aR1 ligands for which adverse anaphylactic-like effects are minimized or avoided completely.

Conclusion

The interest on complement receptor pharmacology and their potential as therapeutic targets is increasingly recognized (16, 56, 71, 83). Specifically, there is pharmaceutical potential for C3aR1 to be a therapeutic target, while working alongside the biomarkers C3a and TLQP-21 for diseases. Detailing the transducerome of C3aR1 enabled us to demonstrate that this GPCR primarily couples to Gi/o/z subtypes to elicit cAMP inhibition and calcium flux, and also recruit β-arrestin to induce internalization. Using this information, we show that TLQP-21 shows a preference for Gi/o-signaling and that SB290157 shows functional antagonism due to potent β-arrestin and internalization. We demonstrate this in cell lines having high translational relevance for human metabolic and inflammatory diseases. Our results, along with the recent release of the structure of C3aR1 (84), and structure-function data (85) relevant for receptor internalization and signaling bias, have relevance toward future C3aR1 drug discovery.

Experimental procedures

Cell lines

HEK 293T cells (ATCC CRL-11268; 59,587,035; certified and tested to be *mycoplasma* free) were cultured in Dulbecco's Modified Eagle Medium (DMEM) containing 10% fetal bovine serum (FBS, Invitrogen) and 0.5% penicillin/streptomycin. Cells were maintained in a humidified incubator at 37 °C and 5% CO_2.

3T3-L1 cells were obtained from ATCC (ATCC, CL-173; certified and tested to be *mycoplasma* free). C3aR1 knockdown (KD) cells were previously described and validated (31). 3T3-L1 cells were plated on 6-well plates and maintained in DMEM supplemented with 10% fetal calf serum (FCS) (Lonza) and with 100 units/ml of penicillin/streptomycin (Invitrogen) in a humidified atmosphere of 5% CO2 at 37 °C. Media was changed on alternate days (∼48 h) until cells were confluent. Once confluent, differentiation into adipocytes was initiated by using a differentiation cocktail containing 10% fetal bovine serum (FBS) (Atlas), 0.5 mM methylisobutylxanthine (Sigma Aldrich), 10 mg/ml insulin (Sigma Aldrich), and 0.25 mM dexamethasone (Sigma Aldrich). After 48 h, the media was refreshed with DMEM supplemented with 10% FBS and 10 mg/ml insulin, which was removed after 48 h. The differentiated cells were maintained in DMEM with 10% FBS and media changed every other day until used in experiments 8 to 9 days after induction.

BV2 cells, a mouse microglia-derived cell line (58) was provided by Dr Vulchanova, UMN. Cells were tested to be *mycoplasma* free, cultured in DMEM supplemented with 10% fetal bovine serum (FBS) (Atlas) and with 100 units/ml of penicillin/streptomycin (Invitrogen) in a humidified atmosphere of 5% CO2 at 37 °C.

LAD2 cells, a human mast cell line (59) was provided by Dr Metcalfe, NIAID. Cells were tested to be *mycoplasma* free, cultured in serum-free media (StemPro-34; Invitrogen) supplemented with 2 mM l-glutamine, 100 IU/ml penicillin, 50 μg/ml streptomycin, and human SCF (100 ng/ml) (R&D systems). Cells were maintained in a humidified atmosphere of 5% CO2 at 37 °C.

Peptides and drugs

mTLQP-21 and R21A peptides were synthesized as previously described (50). $C3a_{63\text{-}77,}$ corresponds to the WWGKKYRASKLGLAR analogue of the C-terminal 15 amino acids of C3a, was purchased from AnaSpec. WWGKKYRASKLGLAR, has been used as receptor-specific probe of C3a activity, and confirmed to be a useful compound for investigating C3a function and physiology (48). SB290157 was purchased from Sigma-Aldrich, PTX was purchased from Cayman, Pitstop-2 was purchased from Abcam, Barbadin was purchased from Axon Medchem, and SKF-96365 was purchased from Tocris.

Bioluminescence resonance energy transfer (BRET) assays

To measure C3aR1-mediated Gα dissociation, HEK293T cells were co-transfected in a 1:1:1:1 ratio of Gα-Rluc8, Gβ1, GFP_2-Gγ, and C3aR1, respectively. After at least 24 h, transfected cells were plated in poly-lysine coated 96-well white clear bottom cell culture plates with DMEM containing 1% dialyzed FBS at a density of 40 to 60,000 cells per 200 μl per well and incubated overnight. This procedure was repeated for other Gαi2, Gαi3, GαoA, GαoB, Gαz, GαsShort, GαsLong, Gαolf, Gαq, Gα11, Gα12, Gα13, Gα14, Gα15 to complete a full screen (47). G protein dissociation $BRET^2$ assays utilized 10 uL of the RLuc substrate coelenterazine 400a (Nanolight, 5 μM final concentration), incubated for 15 min, and read for luminescence at 400 nm and fluorescent GFP_2 emission at 515 nm for 1 s per well using a Mithras LB940. Drug were prepared at (3×) in drug buffer (1× HBSS, 20 mM HEPES, 0.1% BSA, 0.01% ascorbic acid, pH 7.4) and added in duplicate on a 96 well plate and incubated at 37 °C for 60 min. The ratio of GFP_2/Rluc8 was calculated per well and plotted as a function of drug concentration using log (agonist) *versus* response in Graphpad Prism 5 (Graphpad Software Inc).

To measure C3aR1-mediated β-Arrestin2 recruitment, HEK293T cells were co-transfected in a 1:3:15 ratio with C3aR1 containing C-terminal renilla luciferase (RLuc8), GRK2, and Venus-tagged N-terminal β-arrestin2 or Venus-tagged N-terminal β-arrestin1, similar to the protocol found in (86). After at least 24 h, transfected cells were plated in poly-lysine coated 96-well white clear bottom cell culture plates in plating media (DMEM containing 1% dialyzed FBS) at a density of 40 to 60,000 cells in 200 μl per well and incubated overnight. Next day, media was decanted, and cells were washed twice with 60 uL of drug buffer (1× HBSS, 20 mM HEPES, 0.1% BSA, 0.01% ascorbic acid, pH 7.4), then 60 uL of drug buffer was added per well. Drug stimulation was performed with addition of 30 uL of drug (3×) per well and incubated for at various time points. At 15 min before reading, 10 uL of the RLuc substrate, coelenterazine h (Promega, 5 μM final concentration) was added per well, and plates were read for both luminescence at 485 nm and fluorescent Venus emission at 530 nm for 1 s per well using a Mithras LB940. Plates were read for multiple time points up to 60 min at 37 °C after drug addition. The BRET ratio of Venus/RLuc8 was calculated per well and the net BRET ratio was calculated by subtracting the Venus/RLuc8 per well from the Venus/RLuc ratio in wells without Venus-β-Arrestin present. The net BRET ratio was plotted as a function of drug concentration using Graphpad Prism 5 (Graphpad Software Inc).

Gi/o-mediated cAMP inhibition Glosensor assay

To measure Gαi/o-mediated cAMP inhibition, HEK293T cells were co-transfected in a 1:1 ratio with receptor and a split-luciferase-based cAMP biosensor (Glosensor; Promega). After at least 24 h, transfected cells were plated in poly-lysine coated 384-well white clear bottom cell culture plates with DMEM containing 1% dialyzed FBS at a density of 15,000 cells per 40 μl per well and incubated at 37 °C, 5% CO2 overnight. For controls, some were plated with pertussis toxin at a final concentration of 100 ng/uL. On the day of assay, drug dilutions were prepared in filtered fresh assay buffer (20 mM HEPES, 1× HBSS, 0.1% BSA, 0.01% ascorbic acid, pH 7.4) at 3× and 10 μl per well was added to cells containing 20 μl per well of assay buffer. After plates were allowed to incubate with drug for 15 min, 10 μl per well of 1 μM (final concentration) forskolin or 0.3 μM (final concentration) isoproterenol and Glosensor substrate was added. Luminescence counts per second (LCPS) were quantified after 15 min using a Microbeta TriLux microbeta (PerkinElmer) luminescence counter. LCPS was plotted as a function of drug concentration and normalized to % $C3a_{63\text{-}77}$ with 100% as the C3a63 to 77 cAMP inhibition E_{max} and 0% as the forskolin- or isoproterenol-stimulates cAMP baseline. Data were analyzed using log (agonist) *versus* response in GraphPad Prism 5.0 (Graphpad Software Inc).

ELISA surface expression assays

To measure C3aR1-mediated β-Arrestin2 internalization, HEK293T cells were co-transfected in a 1:3:15 ratio of FLAG-tagged-C3aR1, GRK2, and human β-arr2 and incubated at 37 °C, 5% CO2, overnight. After 24 h, transfected HEK293T cells were plated in poly-lysine coated 96-well white clear bottom cell culture plates with DMEM containing 1% dialyzed FBS at a density of 40,000 cells per 200 μl per well and incubated at 37 °C, 5% CO2 overnight. After 24 h, media was decanted, blotted, and 60 μl per well of DMEM media without phenol red (VWR) was pipetted into each well of the plate and then incubated at 37 °C, 5% CO2 for 1 h. Drug dilutions in drug buffer (1× HBSS, 20 mM HEPES, 0.1% BSA, 0.01% ascorbic acid, pH 7.4) were added in duplicate 30 μl per well and incubated for 60 min at 37 °C. Afterwards, media was decanted and cells were fixed with 4% paraformaldehyde in PBS and incubated 20 min at RT. Next, plates were washed 3 times with 60 μl/well of PBS (1× PBS, pH 7.4, LifeTech). Plates received 60 μl per well of blocking solution (5% BSA in PBS), at RT for 1 h. Primary antibody anti-FLAG HRP (SIGMA Cat#A8592) was diluted in PBS in a 1/10,000 solution and added to the plates and incubated for 30 min at RT. The plate was then washed 4 times with PBS buffer (LifeTech). After a final wash, the substrate (1:1) (SuperSignal Pico) was added to each well and the plate immediately was read on the Microbeta Trilux (PerkinElmer) luminescence counter. LCPS were plotted as a

function of drug concentration, and analyzed using log (agonist) *versus* response in GraphPad Prism 5.0 (Graphpad Software Inc).

Fluo-4 calcium influx assays

The Fluo-4 was conducted as previously described (31). 3T3-L1 cells were plated at 60% confluency on μ-Slide eight Well ibiTreat dishes previously coated with collagen coating solution (Cell applications Inc). On the second day, DMEM supplemented with 10% FCS was replaced with Hanks' Balanced Salt Solution 1× (GIBCO) and treated with 2.5 μM Fluo-4 AM (Invitrogen) for 30 min. Cells were then washed with HBSS for 30 min, and then replaced with clean HBSS. The dishes were placed on a live cell environmental chamber in a Nikon Ti-E Deconvolution Microscope System with a New Lambda coat anti-reflective coated 20× objective lens. Elements software was used for the measurement and analysis of the assays. Images of individual wells were taken every second for a total of 3 min. After 30 s, the wells were treated. Excluding dose–response experiments, TLQP-21 was used at a concentration of 10 μM for all experiments, while $C3a_{63\text{-}77}$ was used at 100 nM. Uridine-50-triphosphate (UTP) was used as a positive control. For 3T3-L1 cells, the area under the curve of the first 60 s was calculated by first removing the background noise, and then normalizing each cell to their respective basal intensity. For BV2 and LAD2 cells, area under the curve was reduced to 20 s. Each experiment was then normalized to their control and then analyzed by transforming the values to a 0 to 1 range. For inhibitory Fluo-4, cells were pretreated for 1 h doses, and then exposed to ISO and TLQP-21. Assays with PTX had a 16 h pretreatment. Data were analyzed with one-way ANOVA followed by Tukey's multiple comparisons test.

Lipolysis

For lipolysis experiments, 3T3-L1 adipocytes were serum-starved in Krebs–Ringer buffer containing HEPES (KRH buffer) (NaCl at 120 mM; KCl at 4.7 mM; CaCl2 at 2.2 mM; HEPES at 10 mM; KH2PO4 at 1.2 mM; MgSO4 at 1.2 mM; glucose at 5.4 mM) supplemented with 1% fatty acid-free bovine serum albumin (BSA)(Roche) for 30 min or 3 h. Following starvation, the cells were incubated with KRH buffer containing 4% fatty acid free BSA with various treatments. ISO 50 nM, TLQP-21 10 nM to 1 μM, $C3a_{63\text{-}77}$ 10 nM to 1 μM were used as indicated in the figures. For inhibitory lipolysis experiments with SB290157 and JR14a, cells were pretreated for 1 h with doses, and then exposed to ISO and TLQP-21.

In all experiments, lipolysis was measured as the rate of glycerol release into the induction media. Following the incubation period, the media was collected, and then placed in a water bath at 60 °C for 20 min to inactivate any residual enzymatic activity. The induction media was then stored at −20 °C until the glycerol assay was performed. Glycerol concentration in the conditioned media was measured using the Free Glycerol Determination kit (Sigma) in a flat-bottom 96-well plate following the manufacturer's instructions. All samples incubated for 15 min at room temperature prior to measuring the absorbance at 540 OD on a plate reader (Synergy H1, BioTEK). Glycerol content was normalized to total protein content determined by Bradford Assay (Thermo Scientific). The data were normalized to the control response detected in the same experiment and expressed as fold change over controls. Data were analyzed with one-way ANOVA followed by Tukey's multiple comparisons test.

Phagocytosis

BV2 (microglial) cells were plated in 24-well plates at a density of 2.5×10^5 per mL overnight in FBS supplemented DMEM. Medium was changed to serum-free DMEM, and after 30 min, serum-free DMEM with the corresponding treatments were added at a concentration of 1 μM for 30 min. Following treatment, the medium was discarded and replaced with DMEM containing fluorescent microspheres for 90 min. After incubation, cells were washed 3 times with PBS, then fixed with 4% paraformaldehyde and stained with DAPI. Two random fields of view per well were counted for analysis. Data were analyzed with one way ANOVA followed by Tukey's multiple comparisons test.

LAD2 cell degranulation assay

Cultured LAD2 cells were sensitized overnight with biotinylated-human IgE (100 ng/ml) (Millipore) in StemPro-34 SFM medium (Invitrogen) with human SCF (100 ng/ml) (R & D systems). Cells were then washed and resuspended with HEPES buffer (10 mM HEPES pH 7.4, 137 mM NaCl, 27 mM KCl, 0.4 mM Na2HPO4, 5.6 mM glucose, 1.8 mM CaCl2, 1.3 mM MgSO4.) + 0.04% bovine serum albumin at 1 × 104 per well in 96-well plates. The cells were then incubated with various concentrations of $C3a_{63\text{-}77}$, TLQP-21, or SB290517 respectively for 30 min at 37 °C. β-hexosaminidase (β-hex) measurement in cell supernatants and cell lysate was used as the indicator of LAD2 cell degranulation as described (87, 88). Degranulation was calculated as the percentage of ß-hex recovered from the supernatants compared to the total cellular content in duplicate.

Data availability

All data reported in this paper will be shared by the lead contacts upon request.

Supporting information—This article contains supporting information.

Acknowledgments—Drs Dean Metcalfe and Yun Bai, NIAID, are acknowledged for kindly sharing the LAD2 cells and performing the βhex assay. Dr Vulchanova is acknowledged for kindly sharing the BV2 cells. Megin Nguyen is acknowledged to draw the molecular structures in Figure 7.

Author contributions—J. D. M., A. B., M. R., and Y. S. conceptualization. L. J. L., E. I. A., M. M. C., N. G. C., H. A. B., J. D. M., P. R., and J. P. P., and A. B. investigation; P. R., L. J. L., J. D. M., and A. B.

writing–original draft; P. R., L. J. L., J. D. M., and A. B. writing–review and editing.

Funding and additional information—This work was supported by NIH/NIDDK R01DK117504 (A. B.), NIH/NIDDK R01DK102496 (A. B.), Institute for Diabetes Obesity and Metabolism University of Minnesota (2022 Pilot and Feasibility Program) (A. B.), NIH CTSI UL1TR002494 (Office of Discovery and Translation Pharmacological Development grant) (A. B.), and NIH/NIGMS R35GM133421 (J. D. M.). P.R. and J.P.P. are supported by NIH/NIDDK T32DK083250. The content is solely the responsibility of the authors and does not necessarily represent the official views of the National Institutes of Health.

Conflict of interest—The authors declare no conflicts of interest.

Abbreviations—The abbreviations used are: BRET, bioluminescence resonance energy transfer; C3aR1, complement C3a receptor 1; FBS, fetal bovine serum; GPCR, G protein-coupled receptors; GRKs, G protein-coupled kinases.

References

1. Ceddia, R. P., and Collins, S. (2020) A compendium of G-protein-coupled receptors and cyclic nucleotide regulation of adipose tissue metabolism and energy expenditure. *Clin. Sci.* **134**, 473–512
2. Müller, T. D., Clemmensen, C., Finan, B., DiMarchi, R. D., and Tschöp, M. H. (2018) Anti-obesity therapy: from rainbow pills to polyagonists. *Pharmacol. Rev.* **70**, 712–746
3. Weinstein, L. S. (2014) Role of Gsα in central regulation of energy and glucose metabolism. *Horm. Metab. Res.* **46**, 841–844
4. Hilger, D., Masureel, M., and Kobilka, B. K. (2018) Structure and dynamics of GPCR signaling complexes. *Nat. Struct. Mol. Biol.* **25**, 4–12
5. Smith, J. S., Lefkowitz, R. J., and Rajagopal, S. (2018) Biased signalling: from simple switches to allosteric microprocessors. *Nat. Rev. Drug Discov.* **17**, 243–260
6. Preininger, A. M., and Hamm, H. E. (2004) G protein signaling: insights from new structures. *Sci. STKE* **2004**, re3
7. Kobilka, B. K. (2007) G protein coupled receptor structure and activation. *Biochim. Biophys. Acta Biomembr.* **1768**, 794–807
8. Gurevich, V. V., and Gurevich, E. V. (2020) Biased GPCR signaling: possible mechanisms and inherent limitations. *Pharmacol. Ther.* **211**, 107540
9. Violin, J. D., Crombie, A. L., Soergel, D. G., and Lark, M. W. (2014) Biased ligands at G-protein-coupled receptors: promise and progress. *Trends Pharmacol. Sci.* **35**, 308–316
10. Wisler, J. W., Rockman, H. A., and Lefkowitz, R. J. (2018) Biased G protein–coupled receptor signaling. *Circulation* **137**, 2315–2317
11. Manglik, A., Lin, H., Aryal, D. K., McCorvy, J. D., Dengler, D., Corder, G., *et al.* (2016) Structure-based discovery of opioid analgesics with reduced side effects. *Nature* **537**, 185–190
12. Luttrell, L. M., Maudsley, S., and Gesty-Palmer, D. (2018) Translating *in vitro* ligand bias into *in vivo* efficacy. *Cell Signal.* **41**, 46–55
13. Markham, A. (2020) Oliceridine: first approval. *Drugs* **80**, 1739–1744
14. Tan, L., Yan, W., McCorvy, J. D., and Cheng, J. (2018) Biased ligands of G protein-coupled receptors (GPCRs): structure-functional selectivity relationships (SFSRs) and therapeutic potential. *J. Med. Chem.* **61**, 9841–9878
15. Klos, A., Wende, E., Wareham, K. J., and Monk, P. N. (2013) International union of basic and clinical pharmacology. [corrected]. LXXXVII. Complement peptide C5a, C4a, and C3a receptors. *Pharmacol. Rev.* **65**, 500–543
16. Quell, K. M., Karsten, C. M., Kordowski, A., Almeida, L. N., Briukhovetska, D., Wiese, A. V., *et al.* (2017) Monitoring C3aR expression using a floxed tdTomato-C3aR reporter knock-in mouse. *J. Immunol.* **199**, 688–706
17. Sahu, B. S., Nguyen, M. E., Rodriguez, P., Pallais, J. P., Ghosh, V., Razzoli, M., *et al.* (2021) The molecular identity of the TLQP-21 peptide receptor. *Cell Mol. Life Sci.* **78**, 7133–7144
18. Yanamadala, V., and Friedlander, R. M. (2010) Complement in neuroprotection and neurodegeneration. *Trends Mol. Med.* **16**, 69–76
19. Norgauer, J., Dobos, G., Kownatzki, E., Dahinden, C., Burger, R., Kupper, R., *et al.* (1993) Complement fragment C3a stimulates Ca2+ influx in neutrophils via a pertussis-toxin-sensitive G protein. *Eur. J. Biochem.* **217**, 289–294
20. Molteni, L., Rizzi, L., Bresciani, E., Possenti, R., Petrocchi Passeri, P., Ghè, C., *et al.* (2017) Pharmacological and biochemical characterization of TLQP-21 activation of a binding site on CHO cells. *Front. Pharmacol.* **8**, 167
21. Stephens, S. B., Schisler, J. C., Hohmeier, H. E., An, J., Sun, A. Y., Pitt, G. S., *et al.* (2012) A VGF-derived peptide attenuates development of type 2 diabetes via enhancement of islet β-cell survival and function. *Cell Metab.* **16**, 33–43
22. Schraufstatter, I. U., Trieu, K., Sikora, L., Sriramarao, P., and DiScipio, R. (2002) Complement c3a and c5a induce different signal transduction cascades in endothelial cells. *J. Immunol.* **169**, 2102–2110
23. Gupta, K., Subramanian, H., Klos, A., and Ali, H. (2012) Phosphorylation of C3a receptor at multiple sites mediates desensitization, β-arrestin-2 recruitment and inhibition of NF-κB activity in mast cells. *PLoS One* **7**, e46369
24. Vibhuti, A., Gupta, K., Subramanian, H., Guo, Q., and Ali, H. (2011) Distinct and shared roles of β-arrestin-1 and β-arrestin-2 on the regulation of C3a receptor signaling in human mast cells. *PLoS One* **6**, e19585
25. Guo, Q., Subramanian, H., Gupta, K., and Ali, H. (2011) Regulation of C3a receptor signaling in human mast cells by G protein coupled receptor kinases. *PLoS One* **6**, e22559
26. Hsu, B. E., Roy, J., Mouhanna, J., Rayes, R. F., Ramsay, L., Tabariès, S., *et al.* (2020) C3a elicits unique migratory responses in immature low-density neutrophils. *Oncogene* **39**, 2612–2623
27. Hu, J., Yang, Y., Wang, M., Yao, Y., Chang, Y., He, Q., *et al.* (2019) Complement C3a receptor antagonist attenuates tau hyperphosphorylation via glycogen synthase kinase 3β signaling pathways. *Eur. J. Pharmacol.* **850**, 135–140
28. Fairbanks, C. A., Peterson, C. D., Speltz, R. H., Riedl, M. S., Kitto, K. F., Dykstra, J. A., *et al.* (2014) The VGF-derived peptide TLQP-21 contributes to inflammatory and nerve injury-induced hypersensitivity. *Pain* **155**, 1229–1237
29. Cero, C., Razzoli, M., Han, R., Sahu, B. S., Patricelli, J., Guo, Z., *et al.* (2017) The neuropeptide TLQP-21 opposes obesity via C3aR1-mediated enhancement of adrenergic-induced lipolysis. *Mol. Metab.* **6**, 148–158
30. Possenti, R., Muccioli, G., Petrocchi, P., Cero, C., Cabassi, A., Vulchanova, L., *et al.* (2012) Characterization of a novel peripheral pro-lipolytic mechanism in mice: role of VGF-derived peptide TLQP-21. *Biochem. J.* **441**, 511–522
31. Sahu, B. S., Rodriguez, P., Nguyen, M. E., Han, R., Cero, C., Razzoli, M., *et al.* (2019) Peptide/receptor Co-evolution explains the lipolytic function of the neuropeptide TLQP-21. *Cell Rep.* **28**, 2567–2580.e6
32. Alexander, S. P., Christopoulos, A., Davenport, A. P., Kelly, E., Mathie, A., Peters, J. A., *et al.* (2021) The concise guide to pharmacology 2021/22: G protein-coupled receptors. *Br. J. Pharmacol.* **178**, S27–S156
33. Pasupuleti, M., Walse, B., Nordahl, E. A., Mörgelin, M., Malmsten, M., and Schmidtchen, A. (2007) Preservation of antimicrobial properties of complement peptide C3a, from invertebrates to humans. *J. Biol. Chem.* **282**, 2520–2528
34. Sonesson, A., Ringstad, L., Nordahl, E. A., Malmsten, M., Mörgelin, M., and Schmidtchen, A. (2007) Antifungal activity of C3a and C3a-derived peptides against Candida. *Biochim. Biophys. Acta* **1768**, 346–353
35. Coulthard, L. G., and Woodruff, T. M. (2015) Is the complement activation product C3a a proinflammatory molecule? Re-evaluating the evidence and the myth. *J. Immunol.* **194**, 3542–3548
36. Ahmad, S., Bhatia, K., Kindelin, A., and Ducruet, A. F. (2019) The role of complement C3a receptor in stroke. *Neuromol. Med.* **21**, 467–473
37. Litvinchuk, A., Wan, Y. W., Swartzlander, D. B., Chen, F., Cole, A., Propson, N. E., *et al.* (2018) Complement C3aR inactivation attenuates tau pathology and reverses an immune network deregulated in tauopathy models and Alzheimer's disease. *Neuron* **100**, 1337–1353.e5

38. Kanmura, S., Uto, H., Sato, Y., Kumagai, K., Sasaki, F., Moriuchi, A., *et al.* (2010) The complement component C3a fragment is a potential biomarker for hepatitis C virus-related hepatocellular carcinoma. *J. Gastroenterol.* **45**, 459–467
39. Bartolomucci, A., Possenti, R., Mahata, S. K., Fischer-Colbrie, R., Loh, Y. P., and Salton, S. R. J. (2011) The extended granin family: structure, function, and biomedical implications. *Endocr. Rev.* **32**, 755–797
40. Bartolomucci, A., La Corte, G., Possenti, R., Locatelli, V., Rigamonti, A. E., Torsello, A., *et al.* (2006) TLQP-21, a VGF-derived peptide, increases energy expenditure and prevents the early phase of diet-induced obesity. *Proc. Natl. Acad. Sci. U. S. A.* **103**, 14584–14589
41. Jethwa, P. H., Warner, A., Nilaweera, K. N., Brameld, J. M., Keyte, J. W., Carter, W. G., *et al.* (2007) VGF-derived peptide, TLQP-21, regulates food intake and body weight in Siberian hamsters. *Endocrinology* **148**, 4044–4055
42. Guo, Z., Sahu, B. S., He, R., Finan, B., Cero, C., Verardi, R., *et al.* (2018) Clearance kinetics of the VGF-derived neuropeptide TLQP-21. *Neuropeptides* **71**, 97–103
43. Fargali, S., Garcia, A. L., Sadahiro, M., Jiang, C., Janssen, W. G., Lin, W.-J., *et al.* (2014) The granin VGF promotes genesis of secretory vesicles, and regulates circulating catecholamine levels and blood pressure. *FASEB J.* **28**, 2120–2133
44. Doolen, S., Cook, J., Riedl, M., Kitto, K., Kohsaka, S., Honda, C. N., *et al.* (2017) Complement 3a receptor in dorsal horn microglia mediates pronociceptive neuropeptide signaling. *Glia* **65**, 1976–1989
45. Li, X. X., Kumar, V., Clark, R. J., Lee, J. D., and Woodruff, T. M. (2021) The "C3aR antagonist" SB290157 is a partial C5aR2 agonist. *Front. Pharmacol.* **11**, 2241
46. Mathieu, M. C., Sawyer, N., Greig, G. M., Hamel, M., Kargman, S., Ducharme, Y., *et al.* (2005) The C3a receptor antagonist SB 290157 has agonist activity. *Immunol. Lett.* **100**, 139–145
47. Olsen, R. H. J., DiBerto, J. F., English, J. G., Glaudin, A. M., Krumm, B. E., Slocum, S. T., *et al.* (2020) TRUPATH, an open-source biosensor platform for interrogating the GPCR transducerome. *Nat. Chem. Biol.* **16**, 841–849
48. Proctor, L. M., Moore, T. A., Monk, P. N., Sanderson, S. D., Taylor, S. M., and Woodruff, T. M. (2009) Complement factors C3a and C5a have distinct hemodynamic effects in the rat. *Int. Immunopharmacol.* **9**, 800–806
49. Kroeze, W. K., Sassano, M. F., Huang, X.-P., Lansu, K., McCorvy, J. D., Giguère, P. M., *et al.* (2015) PRESTO-Tango as an open-source resource for interrogation of the druggable human GPCRome. *Nat. Struct. Mol. Biol.* **22**, 362–369
50. Cero, C., Vostrikov, V. V., Verardi, R., Severini, C., Gopinath, T., Braun, P. D., *et al.* (2014) The TLQP-21 peptide activates the G-protein-coupled receptor C3aR1 via a folding-upon-binding mechanism. *Structure* **22**, 1744–1753
51. Kenakin, T. (2015) The effective application of biased signaling to new drug discovery. *Mol. Pharmacol.* **88**, 1055–1061
52. Kenakin, T., Watson, C., Muniz-Medina, V., Christopoulos, A., and Novick, S. (2012) A simple method for quantifying functional selectivity and agonist bias. *ACS Chem. Neurosci.* **3**, 193–203
53. Rivolta, I., Binda, A., Molteni, L., Rizzi, L., Bresciani, E., Possenti, R., *et al.* (2017) JMV5656, A novel derivative of TLQP-21, triggers the activation of a calcium-dependent potassium outward current in microglial cells. *Front. Cell. Neurosci.* **11**, 41
54. Beautrait, A., Paradis, J. S., Zimmerman, B., Giubilaro, J., Nikolajev, L., Armando, S., *et al.* (2017) A new inhibitor of the β-arrestin/AP2 endocytic complex reveals interplay between GPCR internalization and signalling. *Nat. Commun.* **8**, 15054
55. Paksoy, A., Hoppe, S., Dörflinger, Y., Horstmann, H., Sätzler, K., and Körber, C. (2022) Effects of the clathrin inhibitor Pitstop-2 on synaptic vesicle recycling at a central synapse *in vivo*. *Front. Synaptic Neurosci.* **14**, 1056308
56. Rowley, J. A., Reid, R. C., Poon, E. K. Y., Wu, K. C., Lim, J., Lohman, R. J., *et al.* (2020) Potent thiophene antagonists of human complement C3a receptor with anti-inflammatory activity. *J. Med. Chem.* **63**, 529–541
57. Cho, K., Jang, Y. J., Lee, S. J., Jeon, Y. N., Shim, Y. L., Lee, J. Y., *et al.* (2020) TLQP-21 mediated activation of microglial BV2 cells promotes clearance of extracellular fibril amyloid-β. *Biochem. Biophys. Res. Commun.* **524**, 764–771
58. Blasi, E., Barluzzi, R., Bocchini, V., Mazzolla, R., and Bistoni, F. (1990) Immortalization of murine microglial cells by a v-raf/v-myc carrying retrovirus. *J. Neuroimmunol.* **27**, 229–237
59. Kirshenbaum, A. S., Yin, Y., Bruce Sundstrom, J., Bandara, G., and Metcalfe, D. D. (2019) Description and characterization of a novel human mast cell line for scientific study. *Int. J. Mol. Sci.* **20**, 5520
60. Ames, R. S., Lee, D., Foley, J. J., Jurewicz, A. J., Tornetta, M. A., Bautsch, W., *et al.* (2001) Identification of a selective nonpeptide antagonist of the anaphylatoxin C3a receptor that demonstrates antiinflammatory activity in animal models. *J. Immunol.* **166**, 6341–6348
61. El Gaamouch, F., Audrain, M., Lin, W. J., Beckmann, N., Jiang, C., Hariharan, S., *et al.* (2020) VGF-derived peptide TLQP-21 modulates microglial function through C3aR1 signaling pathways and reduces neuropathology in 5xFAD mice. *Mol. Neurodegener.* **15**, 4
62. Gorman, D. M., Li, X. X., Lee, J. D., Fung, J. N., Cui, C. S., Lee, H. S., *et al.* (2021) Development of potent and selective agonists for complement C5a receptor 1 with in vivo activity. *J. Med. Chem.* **64**, 16598–16608
63. Pandey, S., Li, X. X., Srivastava, A., Baidya, M., Kumari, P., Dwivedi, H., *et al.* (2019) Partial ligand-receptor engagement yields functional bias at the human complement receptor, C5aR1. *J. Biol. Chem.* **294**, 9416–9429
64. Yang, L. K., and Tao, Y. X. (2017) Biased signaling at neural melanocortin receptors in regulation of energy homeostasis. *Biochim. Biophys. Acta Mol. Basis Dis.* **1863**, 2486–2495
65. Ghamari-Langroudi, M., Digby, G. J., Sebag, J. A., Millhauser, G. L., Palomino, R., Matthews, R., *et al.* (2015) G-protein-independent coupling of MC4R to Kir7.1 in hypothalamic neurons. *Nature* **520**, 94–98
66. Lotta, L. A., Mokrosiński, J., Mendes de Oliveira, E., Li, C., Sharp, S. J., Luan, J., *et al.* (2019) Human gain-of-function MC4R variants show signaling bias and protect against obesity. *Cell* **177**, 597–607.e9
67. Li, X. X., Lee, J. D., Lee, H. S., Clark, R. J., and Woodruff, T. M. (2023) TLQP-21 is a low potency partial C3aR activator on human primary macrophages. *Front. Immunol.* **14**, 1086673
68. Hutamekalin, P., Takeda, K., Tani, M., Tsuga, Y., Ogawa, N., Mizutani, N., *et al.* (2010) Effect of the C3a-receptor antagonist SB 290157 on anti-OVA polyclonal antibody-induced arthritis. *J. Pharmacol. Sci.* **112**, 56–63
69. Grundmann, M., Merten, N., Malfacini, D., Inoue, A. A., Preis, P., Simon, K., *et al.* (2018) Lack of beta-arrestin signaling in the absence of active G proteins. *Nat. Commun.* **9**, 341
70. Li, K., Anderson, K. J., Peng, Q., Noble, A., Lu, B., Kelly, A. P., *et al.* (2008) Cyclic AMP plays a critical role in C3a-receptor mediated regulation of dendritic cells in antigen uptake and T-cell stimulation. *Blood* **112**, 5084–5094
71. Reid, R. C., Yau, M.-K., Singh, R., Hamidon, J. K., Reed, A. N., Chu, P., *et al.* (2013) Downsizing a human inflammatory protein to a small molecule with equal potency and functionality. *Nat. Commun.* **4**, 2802
72. Rizzi, R., Bartolomucci, A., Moles, A., D'Amato, F., Sacerdote, P., Levi, A., *et al.* (2008) The VGF-derived peptide TLQP-21: a new modulatory peptide for inflammatory pain. *Neurosci. Lett.* **441**, 129–133
73. Sarma, J. V., and Ward, P. A. (2011) The complement system. *Cell Tissue Res.* **343**, 227–235
74. Koc, G., Soyocak, A., Alis, H., Kankaya, B., and Kanigur, G. (2021) Changes in VGF and C3aR1 gene expression in human adipose tissue in obesity. *Mol. Biol. Rep.* **48**, 251–257
75. Lisci, C., Lewis, J. E., Daniel, Z. C. T. R., Stevenson, T. J., Monnier, C., Marshall, H. J., *et al.* (2019) Photoperiodic changes in adiposity increase sensitivity of female Siberian hamsters to systemic VGF derived peptide TLQP-21. *PLoS One* **14**, e0221517
76. Mamane, Y., Chung Chan, C., Lavallee, G., Morin, N., Xu, L. J., Huang, J., *et al.* (2009) The C3a anaphylatoxin receptor is a key mediator of insulin resistance and functions by modulating adipose tissue macrophage infiltration and activation. *Diabetes* **58**, 2006–2017
77. Lewis, J. E., Brameld, J. M., Hill, P., Cocco, C., Noli, B., Ferri, G.-L., *et al.* (2017) Hypothalamic over-expression of VGF in the Siberian hamster

increases energy expenditure and reduces body weight gain. *PLoS One* **12**, e0172724
78. Klos, A., Tenner, A. J., Johswich, K. O., Ager, R. R., Reis, E. S., and Köhl, J. (2009) The role of the anaphylatoxins in health and disease. *Mol. Immunol.* **46**, 2753–2766
79. Regal, J. F., and Klos, A. (2000) Minor role of the C3a receptor in systemic anaphylaxis in the Guinea pig. *Immunopharmacology* **46**, 15–28
80. Song, N.-J., Kim, S., Jang, B.-H., Chang, S.-H., Yun, U. J., Park, K.-M., *et al.* (2016) Small molecule-induced complement factor D (adipsin) promotes lipid accumulation and adipocyte differentiation. *PLoS One* **11**, e0162228
81. Lim, J., Iyer, A., Suen, J. Y., Seow, V., Reid, R. C., Brown, L., *et al.* (2013) C5aR and C3aR antagonists each inhibit diet-induced obesity, metabolic dysfunction, and adipocyte and macrophage signaling. *FASEB J.* **27**, 822–831
82. Kashem, S. W., Subramanian, H., Collington, S. J., Magotti, P., Lambris, J. D., and Ali, H. (2011) G protein coupled receptor specificity for C3a and compound 48/80-induced degranulation in human mast cells: roles of Mas-related genes MrgX1 and MrgX2. *Eur. J. Pharmacol.* **668**, 299–304
83. Wang, Y., Liu, W., Xu, Y., He, X., Yuan, Q., Luo, P., *et al.* (2023) Revealing the signaling of complement receptors C3aR and C5aR1 by anaphylatoxins. *Nat. Chem. Biol.* **19**, 1351–1360
84. Yadav, M. K., Maharana, J., Yadav, R., Saha, S., Sarma, P., Soni, C., *et al.* (2023) Molecular basis of anaphylatoxin binding, activation, and signaling bias at complement receptors. *Cell* **186**, 4956–4973.e21
85. Settmacher, B., Rheinheimer, C., Hamacher, H., Ames, R. S., Wise, A., Jenkinson, L., *et al.* (2003) Structure-function studies of the C3a-receptor: C-terminal serine and threonine residues which influence receptor internalization and signaling. *Eur. J. Immunol.* **33**, 920–927
86. Lewis, V., Bonniwell, E. M., Lanham, J. K., Ghaffari, A., Sheshbaradaran, H., Cao, A. B., *et al.* (2023) A non-hallucinogenic LSD analog with therapeutic potential for mood disorders. *Cell Rep.* **42**, 112203
87. Chan, E. C., Bai, Y., Kirshenbaum, A. S., Fischer, E. R., Simakova, O., Bandara, G., *et al.* (2014) Mastocytosis associated with a rare germline KIT K509I mutation displays a well-differentiated mast cell phenotype. *J. Allergy Clin. Immunol.* **134**, 178–187
88. Woolhiser, M. R., Okayama, Y., Gilfillan, A. M., and Metcalfe, D. D. (2001) IgG-dependent activation of human mast cells following up-regulation of FcgammaRI by IFN-gamma. *Eur. J. Immunol.* **31**, 3298–3307